Svetlana V. Gurevich

Lateral self-organization in nonlinear transport systems described by reaction-diffusion equations

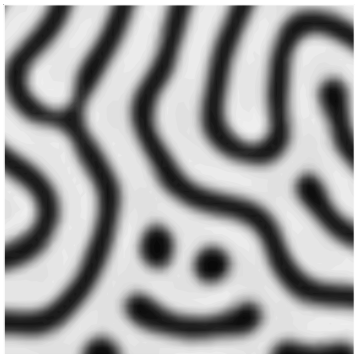

2006

Experimentelle Physik

Lateral self-organization in nonlinear transport systems described by reaction-diffusion equations

Inaugural-Dissertation
zur Erlangung des Doktorgrades
der Naturwissenschaften im Fachbereich Physik
der Mathematisch-Naturwissenschaftlichen Fakultät
der Westfälischen Wilhelms-Universität Münster

vorgelegt von

Svetlana V. Gurevich
aus Sankt-Petersburg

- 2006 -

Dekan:	Prof. Dr. J. P. Wessels
Erster Gutachter:	Prof. Dr. H.-G. Purwins
Zweiter Gutachter:	Prof. Dr. R. Friedrich
Tag der mündlichen Prüfung:	07.02.2007
Tag der Promotion:	07.02.2007

Zusammenfassung

In der vorliegenden Arbeit werden Strukturbildungsphänomene in planaren Gleichspannungs-Gasentladungssystemen mit hochohmiger Barriere auf der Basis von zwei unterschiedlichen Reaktions-Diffusionssystemen mit analytischen and numerischen Mitteln untersucht.

Die Arbeit ist aus drei Teilen zusammengesetzt. Der erste, einleitende Teil gibt einen Überblick über Eigenschaften und Eigenheiten von verschiedenen ein- zwei- und drei-komponentigen Reaktions-Diffusionssystemen, die Strukturbildung in verschiedenen chemischen, biologischen und physikalischen Systemen beschreiben. Außerdem werden eine kurze Einleitung zur Gasentladungsphysik gegeben und die in dem System beobachtenden Strukturen diskutiert.

Der zweite Teil befasst sich mit der Beschreibung des elektrischen Durchbruchs in Townsend-Modus. Durch adiabatische Elimination der Elektronendynamik und Zweiskalen-Entwicklung man kann zeigen, dass die Entladung in diesem Modus durch ein zwei-komponentiges Reaktions-Diffusionssystem qualitativ beschrieben werden kann. Auf dieser Basis werden nichttriviale Lösungen, so genannte Ionisierungsfronten, diskutiert. Insbesondere die Selektion von Frontgeschwindigkeiten in Abhängigkeit von den Anfangsbedingungen wird untersucht.

Im dritten Teil der Arbeit werden lokalisierte Strukturen (so genannte dissipative Solitonen)und Turing-Strukturen in zwei- und drei-komponentigen Reaktions-Diffusionssystemen betrachtet, die eine phänomenologisches Beschreibung des Gasentladungssystems im Glimmmodus darstellen. Die Instabilität der homogenen Lösung, die zur Entstehung von räumlichen Strukturen (Turing-Instabilität) führt und der Einfluss des globalen Rückkoppelungsterms auf die Turing-Instabilität werden diskutiert. Außerdem wird die Stabilität des einzelnes stationären dissipativen Solitons untersucht. Verschiedene typische Destabilisierungsszenarien, wie sowohl laufende und atmende Solitonen als auch deren Kombination, werden mit analytischen and numerischen Mitteln betrachtet.

Abstract

In the present work, pattern-formation phenomena in planar dc gas-discharge system with high-ohmic electrode are investigated analytically and numerically on the basis of two different reaction-diffusion systems.

The work is divided into three parts. The first introductory part briefly overviews properties and peculiarities of different one- two- and three-component reaction-diffusion systems, which describe pattern formation in various chemical, biological and physical systems. In addition, a brief introduction into the gas discharge physics is given and experimental set-up as well as observed patterns are briefly discussed.

The second part deals with a description of electric breakdown in the low-current Townsend mode of discharge operation. Using the adiabatic description of electrons and two-scale expansion one can show that the discharge in this mode is governed by a two-component reaction-diffusion system, which provides a quantitative system description on the macroscopic time scale. On this base ionization fronts being nontrivial solutions of this reaction-diffusion system are discussed in details. In particular, velocity and initial condition selection are investigated in one- and two spatial dimensions.

The third part concerns localized structures (so-called dissipaive solitons) and Turing patterns in two- and three-component reaction-diffusion systems, which are considered as phenomenological models of the experimental system in the glow mode of operation. An instability of the homogeneous solution, leading to the formation of static stationary spatial patterns (Turing instability) is investigated. In addition, the influence of the global feedback in form of an integral term on both instability conditions and the resulting Turing patterns is discussed. Furthermore, stability of a single stationary dissipative soliton is investigated. Several typical destabilization scenarios, such as traveling and breathing solitons as well as their combination, are considered analytically and numerically.

Contents

Introduction **5**

1 Pattern formation in reaction-diffusion systems: an overview **13**
1.1 One-component RD systems 13
1.2 Two-component RD systems 16
1.3 Three- and more-component RD systems 20

2 Physical Background **23**
2.1 Basic definitions and brief history 23
2.2 Classification of discharges in a dc electric field 24
2.2.1 Non-self-sustaining and self-sustaining discharges . . . 24
2.2.2 Conditions for initiating a self-sustaining discharge . 25
2.2.3 Self-sustaining discharge 27
2.3 Experimental system 28
2.3.1 Experimental set-up 28
2.3.2 Experimental results observed in the system 29

I Ionization fronts in planar dc gas-discharge system **31**

3 Two-component RD system in low-current Townsend mode **33**
3.1 The system in question 33
3.2 The gas gap 35
3.2.1 The Townsend solution 37
3.2.2 The perturbation of the Townsend solution 37
3.2.3 The governing equations 39
3.3 The high-ohmic barrier 40
3.4 The reduced system 42

4 Front propagation into an unstable state **45**
4.1 Stationary solutions and their stability 45
4.1.1 Stationary states and ionization waves 45
4.1.2 Uniform solutions 46

4.2 Ionization fronts 47
4.2.1 Ionization fronts in 1D 48
4.2.2 Velocity and initial condition selection mechanism . 54
4.2.3 Ionization fronts in 2D 61

II Localized structures in three-component reaction-diffusion system 65

5 Two- and three-component RD systems: phenomenological modeling 67

6 Stability analysis of steady-state solution 71
6.1 Turing instability in general form 71
6.1.1 Linear stability analysis 72
6.1.2 Activator-inhibitor principe and pattern selection . . 74
6.2 Turing instability in two-component RD system 75
6.3 Turing instability in two-component RD system with an integral term 77
6.3.1 Influence of an integral term 77
6.3.2 Numerical results 78
6.3.3 Experimental observations 81
6.4 Turing instability in three-component system 88
6.4.1 Raus-Gurwitz Stability Criterion 88
6.4.2 Instability criterion for three-component RD system 90
6.4.3 Numerical results 91

7 Localized structures and their stability 95
7.1 General concepts and linear stability analysis 95
7.1.1 Stationary solutions 95
7.1.2 Linear stability analysis 96
7.1.3 Properties of the operator $\mathfrak{L}'(\mathbf{u_s})$ and its spectrum 101
7.2 Destabilization via the mode $n = 0$: Breathing DSs . . . 103
7.2.1 Breathing DSs 103
7.2.2 Amplitude equation in general form 106
7.2.3 Amplitude equation for three-component RD system 109
7.2.4 Numerical results 109
7.3 Destabilization via the mode $n = 1$: Drift-Bifurcation . . 111
7.3.1 Drift-Bifurcation due to a change of time constant 111
7.3.2 Drift-Bifurcation due to a change of shape 115
7.3.3 Experimental observations 116
7.4 Travelling and breathing DSs: codim=2 point 122
7.4.1 One-soliton solution 122

7.5 Multimode destabilization of stationary DS 125

Summary and outlook **129**

List of illustrations used in the introduction **135**

Bibliography **136**

Acknowledgements **157**

Introduction

The Red Queen shook her head,
- You may call it "nonsense" if you like,- she said,-
but I've heard nonsense, compared with which
that would be as sensible as a dictionary!

Lewis Carroll. "Through the looking glass"

The understanding of complex dynamical systems is one of the most important subjects in modern physics. In particular, the spontaneous formation of patterns in the systems far from thermal equilibrium has been the subject of substantial interest over the last decades. Typically these patterns are created by the internal dynamics of the system, this process is called *spatio-temporal self-organization* and is referred to as *pattern formation* [Cross and Hohenberg, 1993, Murray, 1993, Kapral and Showalter, 1995]. The idea that the complex system can increase the inherent order has a long history. One of the earliest statements of this idea was made by the philosopher Descartes in the fifth part of his *Discourse on Method*, where he presents it hypothetically. The ancient atomists believed that the notation of a "intelligent Demiurge" is not necessary, arguing that given enough time and space and matter, organization was ultimately inevitable, although there would be no preferred tendency for this to happen. Descartes added just the idea that the ordinary laws of nature tend to produce organization. Naturalists of the eighteenth century tried to find a kind of "universal laws of form" in order to explain the observed forms of living organisms. Nevertheless, their ideas fell into disrepute until the early twentieth century. The modern understanding is that there are indeed universal laws (arising from fundamental physics and chemistry) that govern growth and form in biological systems.

The term *self-organizing* as such seems to have been first introduced in 1947 by the psychiatrist and engineer W. R. Ashby [Ashby, 1947] and was used thereafter by those associated with general systems theory in the 1960s, but was not accepted in the scientific literature until its adoption by physicists and researchers in the field of complex systems in the 1970s and 1980s. H. Haken established *synergetics* as a new field of research emphasizing the universal character of self-organization and its important properties [Haken, 1983].

Thereafter, pattern formation is essentially a cooperative effect of a distributed system which shows dynamic behavior on selected space and time scales.

Figure 1 shows some typical examples of patterns which can be found in numerous biological, chemical and physical systems. Here we mention only spirals (Fig. 1 (a–c)), stripes (Fig. 1 (d–f)), hexagons (Fig. 1 (g–i)) and localized structures (Fig. 1 (j–l)). The list of illustrations sources used in Fig. 1 is given on page 135. One can see that although the considered systems may have a different nature, the resulting patterns are more or less the same. In many cases it is hard to distinguish patterns taken from different systems. So, one can speak on *the universal character* of pattern formation phenomena. To illustrate this idea we put together a sample list of generic patterns, which is presented below:

- Spirals in two dimensions and scroll waves in three dimensions
  - Galactic arms [Cartin and Khanna, 2002], similar phenomena in plasmas [C. F. Driscoll, 1990];
  - Semiconductors [Rüfer et al., 1980, Gurevich et al., 2003a];
  - Belousov-Zabotinsky reaction, many other chemical examples [Zaikin and Zhabotinsky, 1970, Vanag and Epstein, 2001, Ertl, 1991, Bär et al., 1995];
  - Optical systems [Huneus et al., 2003];
  - Oscillated granular layers [de Bruyn et al., 2001, Jun et al., 2000];
  - Flame propagation [Scott et al., 1997];
  - Bioligy, e.g., cardiac tissue [Fenton and Karma, 1998, Fenton et al., 2002] or bacteria colony growth [Lee et al., 1996, Aranson et al., 1996, Vasiev et al., 1997];
- Stable stationary and travelling nonlinear periodic solutions, e.g., stripes or hexagons
  - Light propagation in a trapping nonlinear media [Arecchi et al., 1999, Rosanov, 2002, Logvin et al., 2000];
  - Crystal growth in two-phase solutions [Kassner, 1996];
  - Granular media, e.g, a rotating or oscillating one. [Hill et al., 1999, Melo et al., 1995];
  - Optical systems [Ackemann and Lange, 2001];
  - Chemistry, e.g., special regimes of Belousov-Zabotinsky [Maini et al., 1997, Sagués and Epstein, 2003] or other chemical reaction [Ouyang and Swinney, 1991];
  - Biology, e.g, animal skin [Murray, 1993, Meinhardt, 1982, Koch and Meinhardt, 1994];

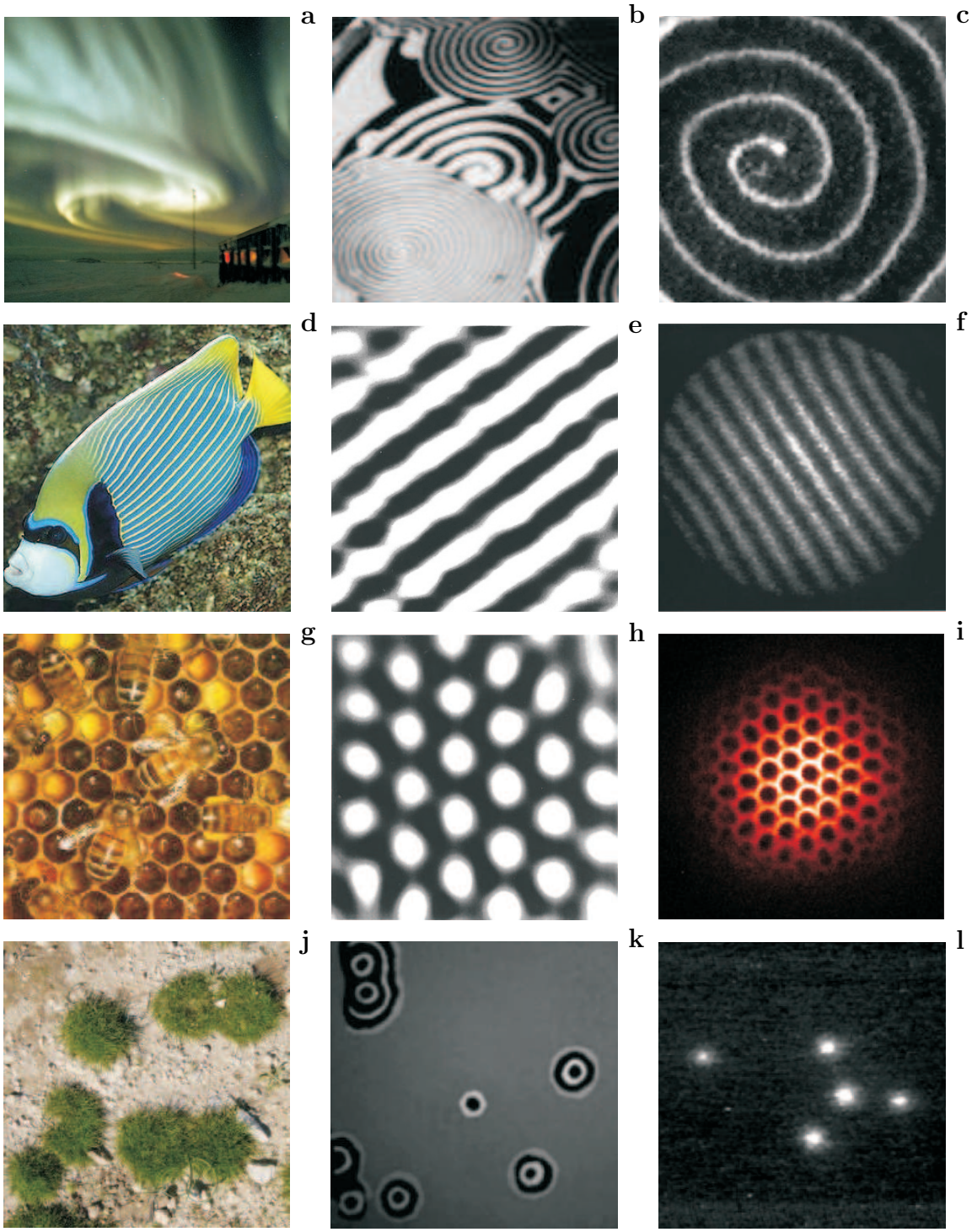

FIG. 1: Self-organized patterns in nature (left column) and in laboratory chemical (middle column) and physical (right column) experiments. Typical examples of spirals (the first row), stripes (the second row), hexagons (the third row) and localized structures (the last row) are shown. (a) a polar light; (b) spiral waves in the catalytic CO-oxidation on Pt(110); (c) spiral pattern in vertically vibrated thin granular layer system; (d) Emperor Angelfish (*Pomacanthus Imperator*); (e) stationary stripes in chlorite-iodide-malonic acid reaction; (f) stripes in two-dimensional gas-discharge; (g) a honeycomb; (h) stationary hexagons in a thin disk shape gel; (i) optical pattern in alkali metal vapors; (j) vegetation pattern: spots of *Poa bulbosa* in the northern Negev; (k) localized spots in BZ reaction dispersed in Aerosol OT-in-oil microemulsion; (l) plasma spots in gas-discharge system.

  - Many other systems, e.g., transversal current structures in electrical discharge, discrete electrical circuits, etc. [Ammelt et al., 1997, Astrov et al., 1996, Zanin et al., 2004];

- Zigzags, labyrinths, etc.
  - Can occur in any system supporting stripes when the latter are destabilized. The type of the structure is determined by the concrete instability [Astrov et al., 1997, Strümpel et al., 2000, Goldstein et al., 1996, Lee and Swinney, 1995];

- Targets, rings, toroidal structures
  - Can occur as a degenerate case in many system supporting spirals waves, see e.g., [Sepulchre and Babloyantz, 1991, Gurevich et al., 2003b, Jun et al., 2000, Desyatnikov and Kivshar, 2001];
  - Biology, in particular growth of bacterial colonies [Murray, 1993, Golding et al., 1998, Dormann et al., 1998];

- Stable stationary and travelling fronts
  - Shocks, where the discontinuity is resolved after the dissipation is taken into account [Whitham, 1999, Landau and Lifshitz, 1999];
  - Phase transitions and phase separation problem [Landau and Lifshitz, 1996];
  - Gunn's effect in semiconductors [Gunn, 1963, Sze, 1997];
  - Chemistry, e.g., combustion [Zeldovich and Frank-Kamenetsky, 1938];
  - Populations spreading in biology [Fisher, 1937, Murray, 1993];
  - Many other systems, e.g., discrete electrical circuits [Purwins and Radehaus, 1988], ionisation waves [Lagarkov and Rutkevich, 1994, Amiranashvili et al., 2005], traffic jams [Whitham, 1999], etc.

- Stable localized solutions, either single and multiply
  - Nonlinear optics, in particular cavity solitons [Arecchi et al., 1999, Rosanov, 2002, Brambilla et al., 2004, Ackemann and Firth, 2005];
  - Semiconductor optical amplifiers [Khitrova et al., 1993, Ultanir et al., 2005];
  - Magneto-optic solitons [Boardman and Xie, 2001, Boardman et al., 2005];
  - Localized wave in binary-fluid convection [Niemela et al., 1990]
  - Stationary localized and oscillatory patterns (oscillons) in BZ reaction dispersed in Aerosol water-in-oil aerosol microemulsion [Vanag and Epstein, 2004];

- Chemical localized spots [Krischer and Mikhailov, 1994, Haim et al., 1996, Sakurai et al., 2002, Mikhailov and Showalter, 2006];
- Solitary structure in granular materials [Umbanhowar et al., 1996];
- Biology, e.g., nerve pulse transmission [Hodgkin, 1951] or vegetation localized patterns [von Hardenberg et al., 2001, Meron et al., 2004];
- Transversal current filaments in gaseous discharge [Müller et al., 1999, Brauer et al., 2000, Strümpel et al., 2001, Astrov and Purwins, 2001].

This is of course only a short list of systems in which self-organized patterns can be found. We have chosen this examples because they can be observed more or less frequently in nature or in laboratory experiments. Remarkable is that although these systems have totaly different nature, in all of them under certain condition one or another pattern can be observed.

Let us give some important features of pattern-forming systems. A necessary condition for self-organization is that the system is permanently far from thermal equilibrium. Therefore the system should be *open*, i.e., continuously exchange matter or energy with its environment [Prigogine, 1969, Haken, 1983]. To this end, a kind of *external driver* should exist. Examples of drivers are voltage sources in different physical systems or flux of chemical reagents. An additional requirement is also *the nonlinearity* of the system. In particular, the system can undergo a qualitative change of its behavior as some *control parameter* is smoothly varied. In other words, *a bifurcation* takes place. The next characteristic feature of pattern-forming systems is the existence of *attractors*, stable states toward which the system evolves. The most simple attractors in such systems represent stationary and time-periodic, i.e., oscillatory states. Notice, that in contrast with the classical solitary waves these stable states will disappear when the driver is switching off. Finally, the pattern-forming system possesses self-organized characteristic length and time scales. Typically, the extension of the pattern is much lager than the size of a individual element of the system, i.e., the system is *spatially extended*. Hence, in order to describe the patterns dynamic, it is often not necessary to take into account the individual dynamics of every single element together with their mutual interactions. Instead, it is possible to interpret the pattern dynamics as a collective phenomenon and describe it by a small set of macroscopic mean-field variables or order parameters. In other words, although there are often different time scales involved in the dynamics of a given system, it is often possible to reduce the number of degrees of freedom by adiabatically eliminating the fast variables [Haken, 1983].

The complexity and variety of self-organizing systems is mathematically reflected by nonlinear equations, which arise in a natural way when systems with many interacting elements, biological systems or chemical reactions are

considered. The framework to describe all these phenomena is provided by the research field called *nonlinear dynamics*. Model equations, describing the main features of patterns are discussed in great details in, e.g., [Cross and Hohenberg, 1993]. One can, e.g., mention (complex) Ginzburg-Landau equation, Swift-Hohenberg equation as well as Kuramoto-Sivashinsky equation. Another example is reaction-diffusion (RD) equations. Equations of this type are widely used to described pattern-formation phenomena in variety of biological, chemical as well as physical systems. Examples are different musters on animal's skin [Gierer and Meinhardt, 1972, Murray, 1993, Koch and Meinhardt, 1994, Meinhardt, 1982], nerve pulse transmission [FitzHugh, 1961, Nagumo et al., 1962], blood clotting [Lobanova and Ataullakhanov, 2003], cardiac tissue [Fenton and Karma, 1998, Fenton et al., 2002], different variants of Belousov-Zhabotinsky reaction and other chemical reactions [Zaikin and Zhabotinsky, 1970, Vanag and Epstein, 2001, Ertl, 1991, Maini et al., 1997] as well as structures, observed in semiconductors [Niedernostheide et al., 1992a, Niedernostheide et al., 1994, Schöll et al., 1998] or gas-discharge systems [Astrov and Logvin, 1997, Kolobov and Fiala, 1994b, Bödeker et al., 2003, Gurevich et al., 2004a, Liehr et al., 2004, Amiranashvili et al., 2005].

This work is focused on reaction-diffusion systems, arising by description of pattern-formation phenomena in planar dc gas-discharge system with semiconductor electrode. This gas-discharge system is considered in two different regimes of operation and two RD systems, specific for each of the operation mode are discussed analytically and numerically. In particular, solitary localized structures, which in case of dissipative systems are refereed to as *dissipative solitons (DSs)* are investigated in details.

The thesis is organized as follows:

- Introduction
  - In Chapter 1 a short review of reaction-diffusion systems and corresponding patterns is given;
  - Chapter 2 gives some basics of gas-discharge physics and the experimental system we are interested in is presented;
- In Part I the planar dc gas-discharge system is discussed analytically and numerically in low-current Townsend operation mode:
  - Chapter 3 demonstrats that the low-current Townsend mode the discharge is governed by a two-component reaction-diffusion system, which provides a quantitative system description on the macroscopic time scale;
  - In Chapter 4 ionization fronts, being the non-trivial solutions of this reaction-diffusion system are discussed in details. Different front types are considered and studied in one- and two spatial dimensions

using analytical as well as numerical methods. In particular, selection of front velocity and initail conditions are discussed;

- Part II deals with the experimental system in glow mode of operation. This situation is much more complicated as compared with that in Part I and we use phenomenological modeling by means of two- and three-component reaction-diffusion systems.

  - In Chapter 6 an instability of the homogeneous solution of a general RD system is discussed. On this base, we investigate formation of static stationary spatial patterns (Turing patterns) in two- and three-component RD systems.
  - In Chapter 7 stability of a stationary DS is investigated. It is shown that by the change of the control parameter a single DS can become unstable. The two destabilizations, caused by the instabilities of first two modes of the corresponding linearization opearator are considered both analytically and numerically. Futhermor, a behavior of the DS in the vicinity of codim $= 2$ point is studied numerically.

- A brief Summary and outlook Chapter closes the thesis.

Chapter 1

Pattern formation in reaction-diffusion systems: an overview

In this chapter a short overview of pattern formation phenomena in different reaction-diffusion systems is given. Various one-, two- and three-component RD systems as well as their solutions are discussed.

As was mentioned in the Introduction, reaction-diffusion (RD) equations arise naturally in systems consisting of many interacting components, (e.g., chemical reactions) and are widely used to describe pattern-formation phenomena in variety of biological, chemical and physical systems. The principal ingredients of all these models are equation of the form

$$\partial_t \mathbf{u} = \mathbf{D}\nabla^2 \mathbf{u} + \mathbf{R}(\mathbf{u}), \tag{1.1}$$

where $\mathbf{u} = \mathbf{u}(\mathbf{r}, \mathbf{t})$ is a vector of concentration variables, $\mathbf{R}(\mathbf{u})$ describes as before a local reaction kinetics and the Laplace operator ∇^2 acts on the vector $\mathbf{u}$ componentwise. $\mathbf{D}$ denotes a diagonal diffusion coefficient matrix. Note that we suppose the system (6.1) to be isotropic and uniform, so $\mathbf{D}$ is represented by a scalar matrix, independent on coordinates.

In the following sections we discuss different nontrivial solutions of this system for different number of components, spatial dimensions as well as different nonlinearities, starting with the case of one component RD system in one spatial dimension.

1.1 One-component RD systems

Investigation in this field starts form the classical papers of Fisher [Fisher, 1937] and Kolmogorov, Petrovsky and Piskunoff [Kolmogorov et al., 1937] motivated by population dynamics issues, where authors arrived at a modified diffusion equation:

$$\partial_t u(x,t) = D\partial_x^2 u(x,t) + R(u), \tag{1.2}$$

with a nonlinear source term $R(u) = u - u^2$. Thereafter the more general reaction function is considered in the literature:

$$R(u) = u - u^n, \quad R(u)|_{u\in[0,1]} \geq 0 \qquad \text{and} \qquad R(0) = R(1) = 0,$$

where, e.g., $R'(0) = 1$.

A typical solution of the Eq. (1.2) is a propagating front, separating two non-equilibrium homogeneous states, one of which is stable and one of which is unstable [Cross and Hohenberg, 1993, Ebert and van Saarloos, 2000, van Saarloos, 2003]. Such fronts behavior is often said to be *front propagation into unstable state* and fronts as such are referred to as *waves (or fronts) of transition from an unstable state*.

Initially the subject was discussed and investigated mostly in mathematical society (see, e.g., [Fife, 1979] where nonlinear diffusion equation was discussed in details). The interest in physics in these type of fronts was stimulated in the early 1980s by the work of G. Dee and coworkers on the theory of dendritic solidification [Dee and Langer, 1983]. Examples of such fronts can be found in various physical [Langer and Müller-Krumbhaar, 1983, van Saarloos et al., 1995], chemical [Showalter and Tyson, 1987, Kapral and Showalter, 1995, Epstein and Showalter, 1996] as well as biological [Britton, 1986, Murray, 1993] systems.

It is known [Aronson and Weinberger, 1978, Ben-Jacob et al., 1985, van Saarloos, 1989] that for such front propagation problems the propagating front always relaxes to a unique shape and velocity, if the initial profile, arising e.g., trough a local initial perturbation, is *steep* enough. Depending on nonlinearities, two regimes of front propagation can be distinguished: To the first front type belongs behavior where the velocity is determined by linearization about the unstable state. Such fronts are called *pulled* or *linear marginal stable*. In the other type, the front propagation is driven by nonlinearities. This regime is referred to as *pushed* or *nonlinear marginal stable* [van Saarloos, 1989, Ebert and van Saarloos, 2000, van Saarloos, 2003]. These and other properties of fronts, propagating into unstable state are discussed in details in Sec. 4.2.

Another important class of one-component RD systems is so-called *bistable systems*. They possess two stable states, say $u = u_1$ and $u = u_3$, separated by an unstable state $u = u_2$. An example of bistable system is the Zeldovich–Frank–Kamenetsky–equation, namely Eq. (1.2) with $R(u) = u(1 - u)(u - \alpha), \alpha \in (0, 1)$, describing the flame propagation [Zeldovich and Frank-Kamenetsky, 1938] as well as switching process in other ZF-like equations, arising some physical, chemical and biological nonlinear media [Svirezhov and Pasekov, 1990, Scott, 2002, Scott, 2003].

The fundamental form of a pattern in bistable infinite one-component media is *a trigger wave*, which represents a propagating front of transition from one stationary state into the other. In the literature other nomenclature,

e.g., *switching waves* is also used. The propagation velocity of a flat front is uniquely determined by the properties of the bistable medium. Indeed, moving to a frame moving with a constant velocity $\xi := x - ct$, and considering partial solution of the form $u = u(\xi)$ one obtains equation

$$Du_{\xi\xi} + cu_{\xi} + R(u) = 0$$

with boundary conditions

$$u(\xi \to -\infty) = u_1, \qquad u(\xi \to +\infty) = u_3.$$

Introducing the function $F(u) = \int\limits_{u_1}^{u} R(s)ds$ one can show that in this situation the velocity of the front can be determined as [Fife, 1979]

$$c = \frac{F(u_3) - F(u_1)}{\int\limits_{-\infty}^{+\infty} (u_{\xi})^2 d\xi}.$$

The numerator of the last equation uniquely defines the velocity direction. In particular, if $F(u_3) = F(u_1)$ the front velocity equals zero, so *stationary front* is also a solution in bistable one-component media. However, the localized states in form of a domain, which can be produced by a connection of two fronts propagating in opposite directions, are normally unstable. Indeed, for the arbitrary choice of parameters one state ($F(u_3)$ or $F(u_1)$) will be dominated. This causes either collapse or expansion of the two-front solution.

In two spatial dimensions the situation is a bit different because corresponding trigger fronts are curved. Moreover, one can show [Fife, 1979, Mikhailov, 1990] that the propagation velocity of a trigger front with the local curvature $\mathrm{K} = 1/\mathrm{R}$ of the front segment is given by

$$c(\mathrm{K}) = c - D\mathrm{K},$$

where c is the propagation velocity of a flat trigger front and R denotes the curvature radius. In particular, this condition implies the modulational stability of a flat front. Namely, if the front line is locally disturbed, the convex part of it will move more slowly than the concave ones, so the distortion will be smoothed out. In three dimensional space the fronts behavior is similar.

As we mentioned above, in one-component RD systems the stationary domains are unstable, i.e., two-front solution collapses or expands. In spite of this problem one consideres a modification of the system introducing the global coupling term by substitution

$$R(u) \mapsto R(u) - C \int udr,$$

where C is a positive constant. Then, when a domain collapses or extends, the global amount of "material" is reduced or increased with respect to previously amount. It was shown, that in such way one can stabilized one domain structure in one-component system [Schimansky-Geier et al., 1991]. However, the integral term mechanism is incapable to stabilize several multidimensional localized structures.

1.2 Two-component RD systems

An essential next step was made in 1952 by Turing [Turing, 1952], who considered a natural and seemingly trivial generalization of Eq. (1.2), namely a two-component system, which can be written without loss of generality in the form

$$\partial_t u(\mathbf{r},t) = D_u \nabla^2 u(\mathbf{r},t) + f(u,v), \tag{1.3}$$

$$\tau \partial_t v(\mathbf{r},t) = D_v \nabla^2 v(\mathbf{r},t) + g(u,v) \tag{1.4}$$

that was associated with diffusing and reacting chemical components. τ represents a dimensionless constant, being the ratio of the characteristic times of the v-component with respect to the that of the u-component. System of such kind can be distinguished by a behavior of a local dynamic of Eqs. (1.3,1.4). The local dynamics is given by the reaction part, i.e. by homogeneous solutions

$$d_t u = f(u,v), \quad d_t v = g(u,v). \tag{1.5}$$

The system

$$f(u,v) = 0, \quad g(u,v) = 0$$

defines so-called *nullclines* of the system. They are curves along which the vector field is either completely horizontal or vertical and represent the set of points when the reaction related change with repect to time of u and v is null. Intersection points $\mathbf{u_0} = (u_0, v_0)$ of all the nullclines are called *the equilibrium points* of the system. These points represent *homogeneous solutions* (or *steady state solutions*) of the original system (1.3, 1.4).

Typically one distinguish bistable, excitable, and oscillating systems. Examples of such systems for reaction functions $f(u,v) = \lambda u - u^3 - v + \kappa_1$, $g(u,v) = (u-v)/\tau$ are presented in Fig. 1.1. Figure 1.1 (a) shows an example of *a bistable* system. In this case, as well as in one-component RD system the system possesses two stable homogeneous states separated by an unstable state. In Fig. 1.1 (b) the system has only one stable state. Such systems are said to be *excitable*. However, when the nullclines intersect as in Fig. 1.1 (c), so that the slope of the nullcline $d_t u = 0$ at the point (u_0, v_0) is less than the slope of the nullcline $d_t v = 0$, the behavior of the system depends on the ratio $\varepsilon = 1/\tau$. If $\varepsilon \ll 1$ the steady state is unstable and is *oscillatory*. For larger values of ε, however, the state $\mathbf{u_0}$ may becomes stable.

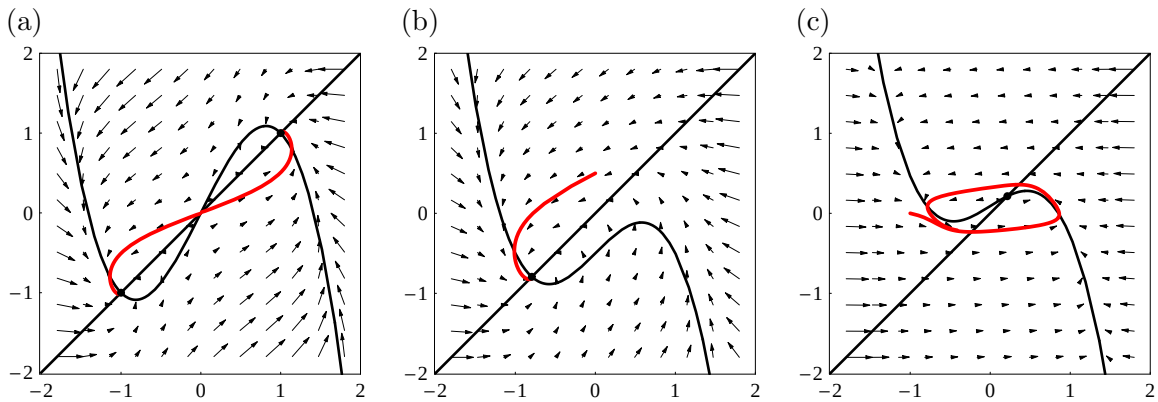

FIG. 1.1: Nullclines and phase space plots of the reaction functions $f(u,v) = \lambda u - u^3 - v + \kappa_1$, $g(u,v) = (u-v)/\tau$. (a) bistable regime, $\lambda = 2$, $\kappa_1 = 0$, $\tau = 1$; (b) excitable regime, $\lambda = 1$, $\kappa_1 = -0.5$, $\tau = 1$; (c) oscillatory regime, $\lambda = 0.625$, $\kappa_1 = 0.09$, $\tau = 10$. The red lines correspond to the solutions of local dynamic (1.5).

Note that depending on the reaction function, other behavior of the local system is also possible. Typical example is front propagation into unstable state, which can be considered in two-component RD system as well. As examples ionization fronts in planar gas-discharge system [Amiranashvili et al., 2005] or planar streamer fronts [Ebert et al., 1996, Ebert and van Saarloos, 1997] can be mentioned.

Apart from the behavior of the equilibrium points of the local system, one can classify them by the signs of the Jacobi matrix components

$$\mathbf{A} = (\partial \mathbf{R}/\partial \mathbf{u})_{\mathbf{u}=\mathbf{u_0}} := \begin{pmatrix} f_u & f_v \\ g_u & g_v \end{pmatrix}.$$

In particular, the most interesting nontrivial dynamics of the system occurs if f_u and g_v have different signs. If, e.g., in some region on the (u,v) plane $f_u > 0$ and $g_v < 0$ the u component calls *an activator* whereas the v component is said to be *an inhibitor*. In addition, if e.g., $f_v < 0$ and $g_u > 0$, then neglecting nonlinear contributions, an increase in activator concentration u results in the growth of both components, whereas growth of the inhibitor component v causes the opposite process. The corresponding class of reaction-diffusion systems possessing this feature is called *activator-inhibitor systems* thereafter (see also section 6.1 for details).

Turning back to Turing, he has found that the steady state $\mathbf{u_0}$ can be stable within the framework of the local dynamics, i.e., within a system (1.5), but unstable due to diffusion. This was a surprising observation because normally one expects that diffusive terms lead to a stabilization of the homogeneous distribution. The most unstable perturbation corresponds to a selected wave-vector k_0 and due to the nonlinearity the instability can lead to the for-

mation of a stable spatial structure, typically hexagonal arrays of spots or stripes with a single characteristic space scale $L \sim 1/k_0$, nowadays called *Turing patterns* [Cross and Hohenberg, 1993]. Thus, Turing instability attributes to a new physical mechanism that is due to the introduction of a second component in equations (1.3,1.4). The Turing instability and resulting patterns are discussed in details in Chap. 6.

Note that the spatial patterns emerging from Turing destabilization mechanism are result of instability of homogeneous solution of Eqs. (1.3,1.4). However, if the homogeneous state is stable, the two-component RD system also admits non-trivial solutions in form of localized solitary objects. In context of dissipative systems we refereed to these objects as *dissipative solitons (DSs)*, following references [Christov and Velarde, 1995, Bode and Purwins, 1995, Purwins et al., 2005]. Other nomenclature can also be found in the literature, e.g., autosolitons [Kerner and Osipov, 1994], oscillons in granular media [Lioubashevski et al., 1999] as well as spots [Nishiura et al., 2005] and pulses [Ohta, 2001] in chemical systems. The model (1.3,1.4) allows solutions in the form of many stationary DSs and soliton molecules [Schenk et al., 1998] in more than one spatial dimension. Note, that in the 2D case the inhibitor can be viewed as a local feedback that localizes the corresponding solutions in both dimensions. Moreover, two-component model is also used to investigate single moving DSs, which can be stabilized by a global feedback term [Krischer and Mikhailov, 1994],

$$f(u,v) \mapsto f(u,v) - C\int_{\Omega} u dr.$$

In some cases, the presence of the global feedback term can influence the formation of Turing structures, although conditions of Turing instability are the same. The influence of the integral term on the formation of Turing structures is discussed in details in section 6.3 of Chapter 6.

There are many important concrete systems that belong to the wide class described by the equations (1.3,1.4). Most typical examples of different reaction-diffusion models and typical solutions can be found in Table 1.1.
Of course, the class of two-component systems is much wider as presented in the table and can be expanded if necessary. In spite of the fact that all discussed model systems describe processes in different chemical, biological and physical systems, their solutions are more or less the same: different spatial and oscillatory patterns, concentric and spiral waves as well as stationary DSs or moving DSs in one spatial dimension. So, one can speak about the universal character of pattern formation phenomena. As mentioned above, in two- or three-dimensions single moving DS can be stabilized by a global feedback term. However, one runs into difficulties if one tries to obtain two or more moving DSs. Namely, the global feedback cannot suppress the growth of antisymmetric combinations of the unstable modes of two or more DSs, so that

Model system	Typical nonlinearities	Typical solutions
Brusselator [Lefever et al., 1967]	$f(u,v) = A - (B+1)u + u^2v$, $g(u,v) = Bu - u^2v$, $A, B \geq 0$	limit cycles, Turing patterns, localized structures [Herschkowitz-Kaufman and Nicolis, 1972], traveling waves [Nicolis and Prigogine, 1997] and mesas [Kolokolnikov et al., 2006] in 1D, spatiotemporal chaos [Kuramoto, 1984]; 2D and 3D various spatial Turing patterns, oscillatory instabilities, their combination [de Wit, 1999]
Oregonator [Field and Noyes, 1974]	$f(u,v) = u(1-u) - (Fv+\phi)\frac{u-q}{u+q}$, $g(u,v) = u - v$, $F, \phi, q > 0$	drifting and rotating spiral waves [Goldschmidt et al., 1998, Keener and Tyson, 1986, Zykov and Engel, 2004], inwardly rotating spirals [Vanag and Epstein, 2001], target patterns [Tyson and Fife, 1980], 2D wave segments [Alonso et al., 2001], trigger and phase waves, wave trains, single solitary pulses [Bordiougov and Engel, 2006]
FitzHugh-Nagumo [FitzHugh, 1961, Nagumo et al., 1962]	$f(u,v) = u(1-u)(u-\alpha) - v$, $g(u,v) = \epsilon(u - \gamma v)$, $\epsilon, \gamma \geq 0$	traveling and breathing waves and pulses both stable and unstable in 1D and 2D [Hagberg and Meron, 1998, Haim et al., 1996, Hagberg and Meron, 1994b, Murray, 1993, Schütz et al., 1995, Bode and Purwins, 1995, Or-Guil et al., 2000], 2D stationary localized spots and solitary molecules [Schenk et al., 1998], Turing patterns and oscillatory instabilities in [Hagberg and Meron, 2000], targets and spiral waves in 2D and 3D [Lee, 1997, Karma, 1990, Margerit and Barkley, 2001], spiral turbulence [Hagberg and Meron, 1994a]
Rinzel-Keller [Rinzel and Keller, 1973]	$f(u,v) = H(u-a) - u - v$, $g(u,v) = \mu u - v$, $H(\cdot)$-Heaviside step function, $\mu \geq 0$	1D stationary, traveling and breathing localized structures [Rinzel and Keller, 1973, Koga and Kuramoto, 1980, Kuznetsova and Osipov, 1995], traveling fronts [Zemskov et al., 2000], 2D stationary and breathing spots [Ohta et al., 1989] one- and two-armed rotating spiral waves [Koga, 1995]
Gray-Scott [Gray and Scott, 1983]	$f(u,v) = F(1-u) - uv^2$, $g(u,v) = uv^2 - (F+k)v$, $F, k > 0$	various spatial-temporal structures, self-replication [Pearson, 1993], annihilation, spatio-temporal chaos [Nishiura and Ueyama, 2001], stationary solitary spots in 1D, 2D and 3D [Muratov and Osipov, 2000], moving solitary spots in 1D, self-replication and annihilation, wave propagation in 2D [Muratov and Osipov, 2001] rotating spirals [Muratov and Osipov, 1999]
Gierer-Meinhardt [Gierer and Meinhardt, 1972]	$f(u,v) = a - bu + \frac{u^2}{v}$, $g(u,v) = u^2 - v$, $a, b > 0$	spots, labyrinth patterns, polygonal domains, hexagonal structures [Gierer and Meinhardt, 1972, Koch and Meinhardt, 1994, Meinhardt, 1982], traveling waves [Meinhardt, 1982]

Table 1.1: Examples of typical two-component RD systems and their solutions.

solutions with several moving and interacting pulses do not exist [Schimansky-Geier et al., 1991].

1.3 Three- and more-component RD systems

An alternative approach to the stabilization of a single moving DS in two and three dimensions is the introduction of a second inhibiting component, which has to be fast and strongly diffusive and therefore plays the role of a local feedback. In the limit of an infinite diffusion coefficient and for appropriate boundary conditions, the local feedback transforms into a global feedback, making the local feedback the more general approach. An additional advantage of this approach is the possibility to stabilize multiple moving DSs [Bode and Purwins, 1995, Bode et al., 2002]. Thus, the introducing of the second inhibitor gives a possibility to investigate a random set of localized objects that move and interact with each other, like, e.g., experimentally observed current filaments in a plane discharge [Purwins et al., 2005].

So, we are now in a good position to discuss a natural generalization of the system (1.3–1.4), i.e., via a $N-$component reaction-diffusion system

$$\tau_\alpha \partial_t u_\alpha = d_\alpha^2 \nabla^2 u_\alpha + F_\alpha(u), \qquad 1 \leq \alpha \leq N, \tag{1.6}$$

where $u = (u_1, u_2, \ldots, u_N)$ is a formal vector consisting of N unknown functions. Such a system was intensely investigated in mathematical context [Smoller, 1994]. Multi-component reaction-diffusion systems have practical applications in various complex fields other then ordinary chemical reactions, e.g., blood clotting [Lobanova and Ataullakhanov, 2003], population dynamics [Kan-on and Mimura, 1998], ecology [Baurmann et al., 2003], etc. Especially three-component RD systems have attracted a great deal of attention in recent years. Typically they are extensions of well-known two-component RD systems, and often arises in natural way, e.g, by modeling of different chemical reactions. We mention only three-component Oregonator model, describing photosensitive Belousov-Zhabotinsky reaction [Amemiya et al., 1998, Bordiougov and Engel, 2003], three-component Gray-Scott model of glycolysis [Nishiura et al., 2005] as well as Krischer-Eiswith-Ertl model of CO oxidation on Pt(110) [Krischer et al., 1992]. In addition, three-component RD system arises by description of many biological and physical systems. Examples are a model for intracellular Ca^{2+} [Falcke et al., 2000], a model of blood clotting [Lobanova and Ataullakhanov, 2003], extended FitzHugh-Nagumo model of Dictyostelium amoebae [Aronson et al., 1996] as well as another extended FitzHugh-Nagumo model describing various patterns arising in gas-discharge system [Or-Guil et al., 1998, Bode et al., 2002, Gurevich et al., 2004b,Liehr et al., 2004,Purwins et al., 2005,Suzuki et al., 1995,Nishiura et al., 2003].

A close investigation shows that actually the cited papers consider an "old" set of generic phenomena like Turing patterns, oscillatory instabilities, spirals, etc., but in the context of many reacting components. Sometimes quite fascinating secondary combinations of these objects can be observed, e.g., "twinkling eyes," where oscillating Turing spots are arranged as a hexagonal lattice [Yang and Epstein, 2003], or oscillatory squares and rhombi [Yang et al., 2004]. However, as mentioned above, RD systems with tree- and more components give rise to investigation of random set of localized objects that move and interact with each other.

In this thesis two different reaction-diffusion systems are studied. As is mentioned above, both systems serve as description of pattern formation phenomena in planar dc gas-discharge system with semiconductor electrode operating in two different regimes (see Chapter 2, where a brief introduction into the gas discharge physics is given and the experimental gas-discharge system we are interested in as well as observed patterns are discussed).

The first system is derived from drift-diffusion approximation in the low-current Townsend mode with a help of two-scale expansion. This system has two components and belongs to the class of Fisher equations, that is, possesses one stable and one unstable homogeneous solutions. In addition, all numerical coefficients in the system can be quantitatively calculated, that is, our predictions can be compared with experimental data (for details see Chapter 3). The typical solution of this system is one- or two-dimensional propagating front. Properties of the reduced reaction-diffusion system solutions in low-current Townsend mode are studied in Chapter 4.

The second RD system describes patterns occurring in the glow mode of the discharge operation. This situation is much more complicated as in low-current mode and simplified approach used there cannot be applied. Therefore, phenomenological modeling is used (see Chapter 7 for details). The obtained system is a two-component system with a cubic nonlinearity and an integral term. The system can be considered as an extension of the FitzHugh-Nagumo equation. In this thesis Turing instability in general form is investigated (see Chpater 6, section 6.1) and applied to the two-component RD system without (section 6.2) and with (section 6.3) a global feedback term. However as is mentioned above systems of this type do not support solutions in form of several moving DSs. Therefore, the third component was added phenomenologically [Schenk et al., 1997]. First of all, we investigate spatial patterns occurring in the system as result of Turing instability (section 6.4). Furthermore, single DSs and their possible destabilizations, such as moving, breathing DSs and their combination are considered in Chapter 7. A summary of the RD systems, presented in the thesis, solutions we are interested in as well as chapters, where these phenomena can be found is shown in Table 1.2.

Model type	Number of components	Solutions	Dimension	Chapter
Fisher	2	fronts, propagating into an unstable state;	1, 2	4
FitzHugh-Nagumo	2	Turing instability;	1, 2	6
	$2+\int$	subcritical Turing instability;	1, 2	
	3	super- and subcritical Turing instabilities;	2	
		single DSs, stationary, moving, breathing and their combination, spirals, other complex structures;	2	7

Table 1.2: Summary of the properties of the RD systems, considered in the thesis.

Chapter 2

Physical Background

In this chapter a brief introduction into the gas discharge physics is given and an experimental gas-discharge system we are interested in is presented. In section 2.1 basic definitions and the most important historical facts can be found, whereas section 2.2 provides a brief overview of different discharge regimes. In section 2.3 an experimental set-up as well as patterns observed there are briefly discussed.

2.1 Basic definitions and brief history

The term *gas discharge* is usually related to all phenomena and processes connected with a flow of electric current through ionized gas [Raizer, 1991]. The name *discharge* originates from objects that slowly loose their electrical charge. This effect was first observed as far back as the sixteenth century. Ch. Coulomb proved two hundred years later that the charge leaks through the air but not through the insulation, that is, the gas discharge takes place. The discharge at low air pressures was discovered and studied by Faraday in 1831-1835. This discharge type is now known as *glow discharge*. At the end of the nineteenth century investigations of dilute gas conductivity led J.J. Tomson to the idea that the current in gases is mostly carried by electrons.

The pioneer of gas discharge physics as such is reputed to be a student of J.J. Tomson J.S.E. Townsend. At the beginning of the twentieth century he established the theory of the gaseous breakdown in a uniform electric field and discovered the laws governing impact ionization. The next fundamental contribution was made by I. Langmiur, who in collaboration with L. Tonks has introduced the fundamental physics concept of *plasma* by investigating the gas discharge at low pressures. In addition, he developed plasma investigation methods, including probe techniques for plasma diagnostics.

Nowadays the term "gas discharge" is treated in a more comprehensive sense. It is considered not only as a process of a current flow through a gas, but also as any gas ionization process by the applied electric field [Raizer,

1991]. The electric field can be constant in time, (i.e., dc electric field) as well as alternative. The latter may be low-frequency and pulsed fields, radio-frequency fields, microwave and even optical fields. In the following, we are concentrated on the case of dc electric fields, although our results can be partly applied to, e.g., pulsed discharges, if the pulse duration is longer than the discharge-formation time.

2.2 Classification of discharges in a dc electric field

2.2.1 Non-self-sustaining and self-sustaining discharges

Discharges in a dc electric field can be classified into *non-self-sustaining* and *self-sustaining* types. Note that gases under standard conditions consist essentially of neutral atoms and molecules and in principal are insulators; therefore no appreciable electric current can flow through. Only ionized gases, i.e., gases containing free charges can act as conductors. In these gases the role of charge carriers is played by positively and negatively charged ions and electrons. Ionization in gases can arise as result of UV light, cosmic rays, or collision of gas atoms with electrons and other particles, where the electron energy exceeds ionization potential of the gas atoms.

Let us suppose that the charge carriers in the gas are created only by some external ionization source of high-energy particles. Then the current and consequently the discharge decays as soon as the external source is switched off. This type of discharge is called *non-self-sustaining*. Let us consider a plane gas gap connected to a circuit with a dc power supply. With the voltage increase, the current I increases as well but soon reaches a saturation value and remains almost constant thereafter. This corresponds to the full pulling of the charges, generated by the external ionization source to the electrodes. With considerable further increasing of U the current suddenly increases again. That means that some electrons in the gas gap accumulate enough energy to generate the secondary electrons by ionization, and so electron avalanches arise. That is, *electron multiplication* or *current amplifying* occurs. The value of the electric field for which the multiplication takes place depends on the gas pressure, multiplied by the gas gap width, and gas art. The amplifying results in an increase of the charge carriers concentration to the value, that depends on initial ionization. However, the discharge remains non-self-sustaining.

Nevertheless, when the electric field E reaches a certain threshold E_b the gas conductivity changes rapidly and *a breakdown* takes place. Corresponding voltage U_b is said to be *a breakdown voltage*, $U_b = E_b d$, where d is the gap width. In this case a switching off of the external ionization source does not lead to the discharge decay. The discharge passes into *a self-sustaining* regime; the ionization is now maintained by processes in the discharge itself.

2.2.2 Conditions for initiating a self-sustaining discharge

As noted above the first model of the transition between non-self-sustaining and self-sustaining discharges was put forward by Townsend. The *ionization coefficient* α was introduced by Townsend and is equal to the number of the different electron-ion pairs, generated by one electron per length unit, i.e., ionization rate.

Consider now the ionization process in a plane gap of width d. At a distance x from the origin, (e.g., cathode) in a thin layer of width dx one electron generates $\alpha \cdot dx$ of electron-ion pairs. If the electron flow I_e flows from the cathode it increases on a value $dI_e = I_e \alpha dx$ in this layer. Integration of this equation under condition that α does not depend on x (which is true for small currents, when space charges do not disturb the electric field in the gap) gives:

$$I_e(x) = I_e(0)e^{\alpha x},$$

where $I_e(0)$ denotes the current, flowing from the cathode to the gas gap. One can see that at the anode, i.e., at $x = d$ the current increases by a factor of $e^{\alpha d}$. This is a gas amplifying regime, i.e., electron-ion pairs multiplication happens as result of electron avalanches. However the discharge can still be non-self-sustaining. For example, if the current $I_e(0)$ is created only by an external ionization source, it decays as soon as the external source is switched off. In order to prevent discharge decay, $I_e(0)$ should be supported by the discharge itself, so a form of "a positive feedback" should exist. Such a feedback can be established only due to particle flow, moving in the opposite direction, namely towards the cathode. In the Townsend model these particles are positive ions. In the following only positive ions are taken into account.

The total current flowing through any transverse discharge cross-section $x = const$ is the same. It consists on electronic current and the current of positive ions I_i moving in the opposite direction. Hence $I_i(d) = 0$ and the total current at the anode equals the electronic current $I_e(d)$. The ion current at the cathode $I_i(0)$ is equal:

$$I_i(0) = I_e(d) - I_e(0) = I_e(0)(e^{\alpha d} - 1).$$

Suppose now that each electron that reaches the cathode knocks out on average γ secondary electrons (γ denotes the *secondary electron emission coefficient*, experiments shown, that $\gamma \ll 1$). Then the electron current of these secondary electrons I_2 from the cathode is

$$I_2 = \gamma I_i(0) = \gamma I_e(0)(e^{\alpha d} - 1),$$

and the total current from the cathode $I_e(0)$ consists of the current of the external ionization source I_1 and the current of the secondary electrons I_2:

$$I_e(0) = I_1 + I_2 = I_1 + \gamma I_e(0)(e^{\alpha d} - 1) = \frac{I_1}{1 - \gamma(e^{\alpha d} - 1)}.$$

Therefor the total current through the gas gap I_i becomes

$$I_i = I_e(d) = I_e(0)e^{\alpha d} = \frac{I_1 e^{\alpha d}}{1 - \gamma(e^{\alpha d} - 1)}.$$

By increasing the voltage, i.e., by increase in the electric field, α increases as well and the current grows up. The discharge however remains non-self-sustaining, as by switching off of the external ionization source ($I_1 = 0$) the total current becomes zero. Nevertheless if the field reaches some critical value, the denominator of the last equation goes to zero and the current becomes infinite for any finite value of I_1, and the external source can be neglected. This is a transition from the non-self-sustaining to the self-sustaining discharge, or *onset of the breakdown*. The condition by which the breakdown takes place is said to be *the Townsend condition* and can be written as:

$$\gamma(e^{\alpha d} - 1) = 1. \tag{2.1}$$

The value

$$\mu \equiv \gamma(e^{\alpha d} - 1) \tag{2.2}$$

is called *the multiplication coefficient*. It shows how many ions reach the cathode as result of the passage of one electron coming from the cathode. Condition (2.1) defines the *breakdown voltage* U_b as a function of gap width d, γ and the known function $\alpha(E)$ [Raizer, 1991],

$$\alpha(E) = Ap \exp\left(-\frac{Bp}{E}\right), \tag{2.3}$$

where p is the gas pressure in the gap. The coefficients A and B are gas-dependent constants, which can be found in the literature [Druyvesteyn and Penning, 1940, Raizer, 1991]. Equation (2.3) is a generalization of experimental data, but can also be found analytically [Druyvesteyn and Penning, 1940]. One can substitute Eq. (2.3) into the Townsend condition (2.1) and obtain so-called *Paschen law*, which reveals the dependence of the breakdown voltage on the discharge parameters:

$$U_b = \frac{Bpd}{\ln(Apd) - \ln(\ln(1 + 1/\gamma))}. \tag{2.4}$$

Equation (2.4) has a remarkable property: The voltage drop over the gas gap in the Townsend mode is independent of the discharge current.

In the strict sense if the voltage applied to the electrodes is exactly equal U_b, (i.e., $\mu = 1$) the breakdown cannot be sustained. A negligible "seed" current at the cathode cannot grow to a macroscopic value, which can be considered as a current of the self-sustaining discharge. So, a small *overvoltage* $\delta U = U - U_b$ should occur. It ensures enhanced reproduction of electrons

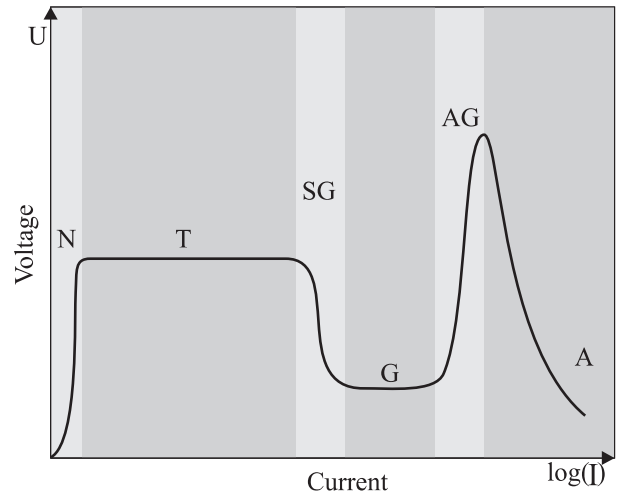

FIG. 2.1: Schematic representation of a gas-discharge CVC. The current I is presented in logarithmic scale. Different discharge modes on the characteristic are marked with grey stripes and denoted as follows: `N`–non-self-sustaining discharge; `T`–Townsend discharge; `SG`–subnormal glow discharge; `G`–glow discharge; `AG`–abnormal glow discharge; `A`–arc discharge.

$\mu > 1$. In this case the ionization and current in the gas will increase until the growth is stopped by recombination or the ohmic resistance Ω of the circuit. As current increases, R_0 accepts a greater part of the power supply voltage $U_{R_0} = I_i R_0$ and the voltage across the electrodes decreases. As this takes place the voltage U drops to the breakdown voltage U_b and the sustained current I_i becomes stationary. Such a self-sustaining discharge is said to be *a Townsend discharge*.

Notice that in the Townsend model the electric field in the gas gap is uniform and is not distorted by space discharges, that is possible only for discharges with a small current.

2.2.3 Self-sustaining discharge

Self-sustaining dc discharges can be further classified with help of the current-voltage characteristics (CVC), which is schematically shown in Fig. 2.1 [Raizer, 1991, Gurevich, 2004]. The form of the CVC strongly depends on the gas type, the gas pressure and the distance between electrodes (strictly speaking, it depends on the $p \cdot d$ product). The CVC starts in the region `N` which corresponds to the non-self-sustaining discharge. This region can be characterized by an extremely low discharge current, which is caused by a simple drift of the charge carriers in the electric field (see subsection 2.2.1 for details). As soon as the voltage applied to the discharge reaches the breakdown voltage U_b the self-sustaining discharge takes place, which at the whole horizontal line `T` corresponds to *the Townsend discharge* (see subsection 2.2.2).

As mentioned above, in the Townsend regime the electric field is uniform due to small currents and absence of a noticeable space charge. However at a higher discharge current the field redistributes after the breakdown and is almost completely concentrated near the cathode. It occurs because of the generation of the positive space charge near the cathode due to the ion current (electron current near the cathode is small compared to the ion current). Moreover, the considerable part of the gas gap goes into the state with a high electrical conductivity and a so-called *positive column* is formed. So almost all the applied electric field is localized in the cathode area, occupied with the space charge. Hence almost all voltage applied to the gap drops in this layer, which is referred to as *the cathode layer*. This voltage is approximately equal to the minimal breakdown voltage for the cathode layer gap width. In such a way the Townsend condition is fulfilled for far less voltages, than for the uniform gap field. This type of the discharge is called *glow discharge*. It is marked as `G` in Fig. 2.1, whereas the transition region between `T` and `G` with a negative differencial resistivity is called *the subnormal glow discharge* (see `SG` area in Fig. 2.1) In the glow discharge mode the discharge current is normally not spread on the electrode surface, but is constricted and forms a filament (or "current spot"). An increase in the discharge current results in an increase in the area of the spot while the current density remains constant.

When the area of the current spot exceeds the electrode area, the discharge can occupy the backside of the electrodes, and the gap voltage increases, as shown in Fig. 2.1 as `AG` . This is the *abnormal glow discharge*. In this discharge mode the gap voltage increases while increasing the discharge current, and thus the power dissipated in the discharge increases. This causes the electrode to be heated to temperatures at which the thermoelectron emission mechanisms start playing a key role. These mechanisms are more effective than the γ-processes; thus in this case the gas discharge does not require such a high voltage drop over the cathode layer to maintain the self-sustained discharge. The gap voltage in this mode falls down to some tens of volts, but the power dissipation in the discharge stays high because the discharge conductivity is low and the current is high. This discharge mode is called the *arc discharge*, and is marked as `A` in Fig. 2.1.

2.3 Experimental system

2.3.1 Experimental set-up

The experimental set-up that underlies the theories in this thesis is a planar dc gas-discharge system with a high-ohmic barrier. The system consists of the gas-discharge cell, vacuum system, cryothermostat and electric circuit. The

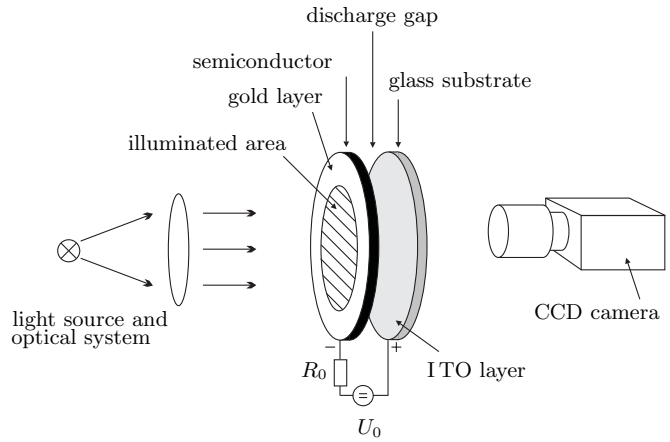

FIG. 2.2: Schematic plot of the experimental set-up. Explanations are given in the text.

discharge takes place in the discharge cell, which consists of two plain-parallel electrodes with a gas gap between them (see Fig. 2.2). The gas gap width d can be varied between $0.1 - 2$ mm. It can be filled with different atomic or molecular gases, typically it is nitrogen (N_2), helium (He) or argon (Ar) at pressures of $p \approx 30 - 400\,\mathrm{hPa}$. The electrodes of the gas-discharge system are a low-ohmic anode and a high-ohmic semiconductor cathode of $0.5 - 1.5$ mm width, contacted from one side with a semitransparent metallic layer (e.g., gold). As the semiconductor cathode one can use different wafers, e.g., silicon wafers doped with platinum (Si⟨Pt⟩) or zinc (Si⟨Zn⟩), semi-insulating gallium arsenide wafers ((si)-GaAs) as well as semi-insulating gallium arsenide wafers doped with chromium ((si)-GaAs⟨Cr⟩). The specific resistivity of the semiconductor takes values of $\rho_{\mathrm{SC}} \approx 10^7 - 10^8\,\Omega \cdot \mathrm{cm}$ and can be controlled via the internal photo effect by illumination. Typically the semiconductor is either cooled to $T = 100\,K$ or has a room temperature ($T \simeq 300\,K$). The anode is a thin, transparent to visible light, conductive layer of indium tin oxide (ITO), evaporated onto both sides of the glass substrate. The system is supplied with an external voltage U_0 of several kV, whereas the global current may be limited by a series resistor R_0 of several MΩ. The luminance distribution in the discharge gap is known to be locally proportional to the current density distribution [Ammelt et al., 1997] and can be recorded through the ITO electrode by a charge-coupled device (CCD) camera. Altogether, the experimental set-up is very similar to a version of the system that is used as an ultrafast converter of infrared images to the visible ones [Portsel et al., 1999].

2.3.2 Experimental results observed in the system

As shown above the experimental system in question can be characterized by a number of physical quantities. One distinguishes between quanti-

ties, which can be controlled (so called *control parameters*, e.g., gas pressure, specific resistivity of the semiconductor or supply voltage) and whose, which become *self-organized* during the experiments, e.g., the discharge luminance or current density.

When the chosen control parameter, (e.g., supply voltage U_0) is increased beyond some threshold, (e.g., ignition voltage), various forms of spatially inhomogeneous self-organized luminance patterns can be observed. Notice that depending on the shape of the current-voltage characteristics of the semiconductor pattern formation can take place either in gas-discharge gap or in semiconductor. In this thesis we are interested in patterns, occurring in the gas gap. We mention only spiral and target patterns [Gurevich et al., 2005, Astrov et al., 1998], stripes and hexagons [Astrov et al., 1997, Ammelt et al., 1997, Ammelt et al., 1998], as well as current spots [Strümpel et al., 2001, Astrov and Purwins, 2001, Liehr et al., 2004].

However, despite of good knowledge of microscopic underlaying processes, the observed macroscopic patterns are not understood to large extent. One reason is that typically the current spots are 3D objects that evolve on a time scale of a millisecond or longer. In contrast, the smallest time scale that should be taken into account in drift-diffusion approximation, is an electron travel time that is of the order of 10 nanoseconds for the system in question. That is, a direct numerical solution of the plasma transport equations is therefor very time consuming or even impossible. The alternative is to develop an appropriate reduced discharge model.

In this thesis, a planar dc gas discharge system operating in the low-current Townsend mode is studied analytically and numerically in Part I, whereas in Part II the behavior of the system in glow mode of operation, in terms of phenomenological modeling is discussed.

Part I

Ionization fronts in planar dc gas-discharge system

Chapter 3

Two-component RD system in low-current Townsend mode

In this chapter electric breakdown and ionization fronts are considered theoretically in a sandwich-like dc discharge system. Using the adiabatic description of electrons and two-scale expansion we demonstrate that in the low-current Townsend mode the discharge is governed by a two-component reaction-diffusion system, which provides a quantitative system description on the macroscopic time scale.

3.1 The system in question

The schematic geometry of the discharge cell in question is shown in Fig. 3.1 (see also section 2.3.1 for details). The gas layer is located parallel to the (x, y) plane and extends from $z = 0$ to $z = d$ in z-direction. The current is essentially parallel to z-axis. The cathode consists of a high-ohmic barrier located at $d < z < d + d_c$. Two planar metal contacts are located at $z = 0$ (anode) and $z = d + d_c$. Both d and d_c are considerably smaller than the radius of the discharge cell. Consequently, the x and y dependence of the electric potential and particle densities is assumed to be weak compared with the z dependence. Nevertheless, the radial dependence cannot be ignored completely, as it is responsible for the laterally extended pattern we are interested in.

Now we consider the development of electric breakdown in Townsend mode and look for peculiarities resulting from the high-ohmic barrier. Let us assume that by proper choice of the supply voltage the system is prepared to operate near the breakdown point. That is, the voltage applied to the gas almost equals the Townsend breakdown voltage U_b. In this mode of operation the current is negligible and is often localized in several narrow channels caused by unavoidable inhomogeneities in the system. The channels serve as seed current fluctuations for the breakdown. The supply voltage is then suddenly increased

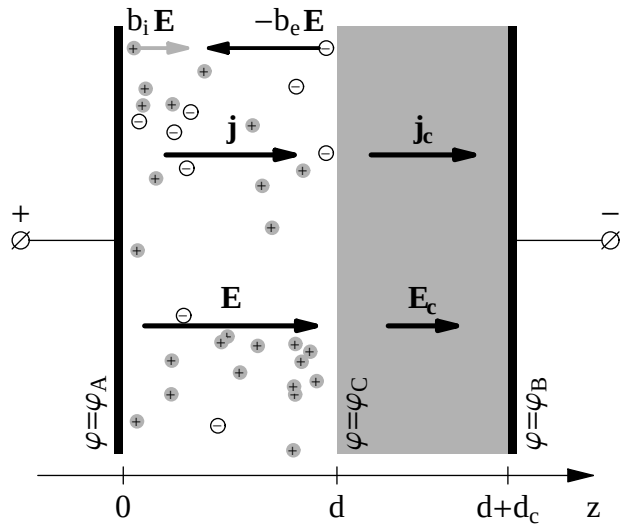

FIG. 3.1: A cross-section of a typical planar discharge cell consisting of a metal anode, a gas layer, a high-ohmic cathode, and another metal contact. φ_A(t), $\varphi_C(x, y, t)$, and $\varphi_B(t)$ are potentials at $z = 0$, $z = d$, and $z = d + d_c$. $\mathbf{E}$ and $\mathbf{E}_c$ denote the axial electric field in the gas and in the high ohmic cathode, $\mathbf{j}$ and $\mathbf{j}_c$ are the corresponding current densities. Drift velocities of electrons and ions, as expressed by mobilities $b_{e,i}$, are schematically shown at the top. Both d and d_c are typically several fractions of a mm, whereas the radial space scale is several centimeters.

to a larger value U_s such that

$$U_s - U_b \ll U_b. \tag{3.1}$$

In this situation system parameters such as diffusion and mobility coefficients for electrons and ions are not changed whereby the ionization coefficient varies considerably due to the strong dependence on the electric field. Note that in many experiments with the high-ohmic barrier the difference $U_s - U_b$ is several tens of volts, whereas U_b is several hundreds of volts [Gurevich et al., 2003a, Gurevich et al., 2005]. Another example is a direct experimental measurement of U_b, where $U_s - U_b$ can approach one volt [Lisovskiy et al., 2000].

Breakdown in a system like Fig. 3.1 transforms it to a new state that is assumed to be in the Townsend mode. In the case that the current density is uniform, it is determined by

$$j = j_0 = \frac{U_s - U_b}{\rho d_c}, \tag{3.2}$$

where ρ is the specific resistivity of the high ohmic barrier. The value of j_0 is assumed to be small enough to allow space-charge effects to be neglected. Typically $j_0 < 10^{-4}\,\mathrm{A/cm^2}$ if the system is on the right-hand-branch of the Pashen curve, and $j_0 < 10^{-2}\,\mathrm{A/cm^2}$ for the left-hand-branch. In this way the

discharge operates in the Townsend mode. The breakdown can be considered as a transition between the states $j = 0$ and $j = j_0$. Our goal is to investigate such a transition.

Inequality (3.1) ensures that the voltage drop $U_{\text{gas}} = \varphi_A - \varphi_C$ at the gas gap is not very different from the breakdown value. Consequently it is natural to present the gap voltage as

$$U_{\text{gas}} = U_b + \delta U(x, y, t), \quad \delta U \ll U_b,$$

where δU is the overvoltage (see Chapter 2). The essential difference from the familiar case of metal electrodes is that in the case of Fig. 3.1 both φ_C and δU can depend on position. The maximal possible overvoltage is achieved if the whole supply voltage is applied to the gas gap, i.e.,

$$\delta U(x, y, t) \leq U_s - U_b, \tag{3.3}$$

where the right-hand-side is a predetermined quantity, whereas the left-hand-side is a dynamical variable to be found.

The major part of the gas electric field $\mathbf{E}$ is directed parallel to the z axis. This axial field component can be presented as

$$E_z = E_b + \delta E, \quad \int_0^d \delta E(x, y, z, t)\, dz = \delta U, \tag{3.4}$$

where $E_b = U_b/d$ is the breakdown field. The radial electric field $\mathbf{E}_\perp$ can be exactly calculated at the gas-electrode interfaces

$$\mathbf{E}_\perp\big|_{z=0} = 0, \quad \mathbf{E}_\perp\big|_{z=d} = \nabla_\perp \delta U,$$

where $\nabla_\perp = (\partial_x, \partial_y)$. The first (anode) equation holds for any metal electrode and the second (cathode) follows from the definition of the overvoltage. Due to the small width of the discharge cell, the intrinsic radial field can be approximated as [Amiranashvili et al., 2005]

$$\mathbf{E}_\perp = \frac{z}{d} \nabla_\perp \delta U, \tag{3.5}$$

the approximation can also be justified by a systematic calculation of the electric field. As ensured by (3.1) and (3.3), both axial and radial distortion of E_b are small. As a result the absolute value of the electric field is always approximated as $E_b + \delta E$.

3.2 The gas gap

In this section we discuss the gas gap where electrons and positively charged particles move in opposite direction as prescribed by the applied electric field. Only one positive charge carrier specie (ions) is considered. The drift velocity of electrons and ions is determined by mobilities $b_{e,i}$

$$\mathbf{v}_e = -b_e \mathbf{E} \quad \text{and} \quad \mathbf{v}_i = b_i \mathbf{E}.$$

There is also a stochastic particle flux described by the diffusion coefficients $D_{e,i}$. Both mobility and diffusion coefficients depend on the local electric field. However, in the Townsend mode they can be assumed to be constant determined by E_b. The particle densities of electrons n_e and ions n_i are governed by two continuity equations

$$\partial_t n_{e,i} + \nabla(n_{e,i}\mathbf{v}_{e,i} - D_{e,i}\nabla n_{e,i}) = S_{e,i},$$

where $S_{e,i}$ is the ionization source-term. The equations can be rewritten in a simpler form

$$\partial_t n_{e,i} + \mathbf{v}_{e,i}\nabla n_{e,i} - D_{e,i}\nabla^2 n_{e,i} = S_{e,i},$$

as the space-charge effect is negligible in the Townsend mode (see Chapter 2 for details).

Let us undertake the following simplifications. We use a local field approximation and write

$$S_e = S_i = \alpha(E) n_e v_e,$$

where the Townsend parameter $\alpha(E)$ describes ionization rate and $E = E_b + \delta E$. Even if very small, δE should be taken into account here because α is a strong function of the electric field. Note that the local field approximation is not a good model in the case that the electric field is subject to drastic changes, e.g., in the cathode fall. In the Townsend mode, however, the field is practically constant and therefore the simple local ionization term is justified. Furthermore, the ion diffusion is completely neglected. We also neglect the electron diffusion in the axial direction (see, e.g., [Raizer and Surzhikov, 1990]). In contrast to this, the radial diffusion of electrons is taken into account. We also keep the radial drift terms for electrons and ions considering them as a small perturbation with respect to the axial drift flux. Finally, we are interested in processes that are slower then the typical ion travel time

$$\tau_i = \frac{d}{b_i E_b},$$

and consequently $\partial_t n_i$ is taken into account as a small perturbation. The dependence of n_e on time is eliminated adiabatically by placing $\partial_t n_e$ at zero.

Altogether, the continuity equations for electrons and ions are rewritten as

$$[b_e\partial_z n_e + b_e\alpha(E)n_e]E_z = -b_e\mathbf{E}_\perp\nabla_\perp n_e - D_e\nabla_\perp^2 n_e, \tag{3.6}$$

$$[b_i\partial_z n_i - b_e\alpha(E)n_e]E_z = -b_i\mathbf{E}_\perp\nabla_\perp n_i - \partial_t n_i, \tag{3.7}$$

where $\nabla_\perp^2$ is the radial part of the Laplace operator. The left-hand-sides of Eqs. (3.6,3.7) provides us with the classical (Townsend) discharge solution; the right-hand-side describes its perturbation due to radial drift, radial electron diffusion and ion inertia.

Of course, appropriate boundary conditions must be imposed on the electrodes. In this context we remember that the diffusion in the axial direction is completely ignored, i.e., the boundary conditions can be taken in the Townsend form [Raizer, 1991]

$$n_i\big|_{z=0} = 0 \quad \text{and} \quad \left.\frac{n_e}{n_i}\right|_{z=d} = \gamma\frac{b_i}{b_e}, \tag{3.8}$$

where γ is the secondary emission coefficient.

3.2.1 The Townsend solution

Our first concern is to reproduce the classical solution for the Townsend discharge [Raizer, 1991]. To this end we ignore the right-hand-sides of Eqs. (3.6,3.7) and replace E by the electric breakdown field E_b. The expressions for the electron and ion densities are

$$n_e = e^{-\alpha_b z} n_0, \tag{3.9}$$

$$n_i = \frac{b_e}{b_i}(1 - e^{-\alpha_b z}) n_0, \tag{3.10}$$

where $\alpha_b = \alpha(E_b)$. The well known additional restriction (2.1)

$$\gamma\left(e^{\alpha_b d} - 1\right) = 1 \tag{3.11}$$

results from the cathode boundary condition and implicitly determines E_b. The parameter n_0 is a constant of integration and can be interpreted as the electron density at the anode; n_0 depends on all space-time variables but z, this dependence is assumed to be slow on the time scale τ_i and space scale d. The electric current density is approximated as

$$j = q b_e E_b n_0, \tag{3.12}$$

is parallel to the z axis, and depends on all variables but z. In (3.12) q is the elementary charge.

It is appropriate to assume that n_0 is the true anode electron density, so that a possible distortion of (3.9) disappears at $z = 0$. A possible distortion of (3.10) disappears at the anode as well, because of the anode boundary condition (3.8). In what follows a dynamical equation for $n_0(x, y, t)$ will be found as a compatibility condition for the next step of the perturbation expansion. It will then be transformed to a more physical equation for the axial current, as given by (3.12).

3.2.2 The perturbation of the Townsend solution

If one takes the right hand sides of Eqs. (3.6, 3.7) into account, Eqs. (3.9, 3.10) are not exact solutions. Therefore we perform the next step

of the perturbation theory and write the particle densities as follows

$$n_e = e^{-\alpha_b z} n_0 + \delta n_e,$$
$$n_i = \frac{b_e}{b_i}(1 - e^{-\alpha_b z}) n_0 + \delta n_i,$$

where the perturbations $\delta n_{e,i}$ originate from the radial drift, electron diffusion, and ion inertia. As explained above, we can assume $\delta n_{e,i} = 0$ at $z = 0$, but not at $z = d$. These densities have to be substituted into Eqs. (3.6, 3.7). A compatibility condition for the resulting equations set is a desired dynamical equation for n_0.

It is profitable to rewrite $n_{e,i}$ in the equivalent form that is suggested by the structure of the Townsend solution. Without loss of generality we introduce $\tilde{n}_{e,i}$ instead of $\delta n_{e,i}$ so that

$$n_e = e^{-\alpha_b z}(n_0 + \tilde{n}_e), \tag{3.13}$$

$$n_i = \frac{b_e}{b_i}(1 - e^{-\alpha_b z})(n_0 + \tilde{n}_e) + \tilde{n}_i, \tag{3.14}$$

where $\tilde{n}_{e,i} = 0$ at $z = 0$. The variable $\tilde{n}_e$ describes the distortion of n_0 whereas $\tilde{n}_i$ is a "non-Townsend" part of the perturbation. Equation (3.13) and the electric field (3.4,3.5) are now inserted into (3.6). Omitting high-order terms we arrive at the equation for the perturbed electron density

$$\partial_z \tilde{n}_e = -z \nabla_\perp n_0 \nabla_\perp \frac{\delta U}{U_b} - \lambda_e \nabla_\perp^2 n_0 - \alpha_b' n_0 \delta E, \tag{3.15}$$

where $\alpha_b' = \alpha'(E_b)$ comes from the Taylor expansion of the ionization coefficient. The parameter

$$\lambda_e = \frac{D_e}{b_e E_b}$$

is recognized as the electron diffusion length. We now integrate (3.15) from $z = 0$ to $z = d$ and arrive at the equation

$$\tilde{n}_e\big|_{z=d} = -\frac{d^2}{2} \nabla_\perp n_0 \nabla_\perp \frac{\delta U}{U_b} - \lambda_e d \nabla_\perp^2 n_0 - \alpha_b' n_0 \delta U, \tag{3.16}$$

which together with (3.13) determines δn_e at the cathode.

In a similar manner we substitute (3.14) into (3.7) to get the following equation for $\tilde{n}_i$

$$\frac{b_i}{b_e} \partial_z \tilde{n}_i = (1 - e^{-\alpha_b z}) \left(\lambda_e \nabla_\perp^2 n_0 - \frac{\tau_i}{d} \partial_t n_0 \right) + \alpha_b' n_0 \delta E.$$

Integration over $0 < z < d$ gives the result

$$\frac{b_i}{b_e} \tilde{n}_i\big|_{z=d} = \left(1 - \frac{1 - e^{-\alpha_b d}}{\alpha_b d} \right) (\lambda_e d \nabla_\perp^2 n_0 - \tau_i \partial_t n_0) + \alpha_b' n_0 \delta U \tag{3.17}$$

together with Eqs. (3.14, 3.16) determining δn_i at the cathode. Note that both δn_e and δn_i contain $\nabla_\perp \delta U$; this term is specific for our problem and disappears for the metal electrodes.

3.2.3 The governing equations

The axial electric field, as given by (3.4), contains the unknown perturbation δE. That is the reason for deriving equations only for the $\tilde{n}_{e,i}$ at $z = d$. This information is however sufficient to determine n_0. We substitute (3.13) and (3.14) in the cathode boundary condition (3.8) to get $\tilde{n}_i\big|_{z=d} = 0$, i.e., the "non-Townsend" part $\tilde{n}_i$ must disappear at the cathode. Equation (3.17) reduces to the compatibility condition

$$\tau_i \partial_t n_0 = \lambda_e d \nabla_\perp^2 n_0 + C_\gamma \alpha_b' n_0 \delta U, \tag{3.18}$$

which is the desired equation for n_0. The familiar inequality $\gamma \ll 1$ was not used in the derivation, nevertheless the numerical factor

$$C_\gamma = \frac{1+\gamma}{1 - \ln^{-1}(1 + 1/\gamma) + \gamma}$$

is of order unity for all reasonable γ values. Equation (3.18) is not closed, as it contains δU. It is of interest to note that the terms containing $\nabla_\perp \delta U$ cancel so that Eq. (3.18) is formally similar to that for the metal electrodes [Kolobov and Fiala, 1994a], where the overvoltage is compensated by diffusion and the radial drift flux is not important. The difference is that in our work δU is a new dynamical variable in a *partial* differential equation to be derived from the consideration of the high-ohmic barrier. Before doing so let us discuss Eq. (3.18) in more details. It is a nonlinear diffusion equation, the corresponding diffusion parameter

$$D_a = \frac{\lambda_e d}{\tau_i} = D_e \frac{b_i}{b_e}$$

is recognized as the ambipolar diffusion coefficient. This fact is not unexpected [Raizer and Surzhikov, 1993, Kaganovich et al., 1994] because the spatial spreading of particles is due to electron diffusion, whereas the typical microscopic time scale for the current is determined by the ion travel time. Equation (3.18) has two uniform stationary solutions either with $n_0 = 0$ (zero current) or with $\delta U = 0$ and $n_0 = \text{const}$, the latter results from the equilibration of j [Eq. (3.12)] and j_0 [Eq. (3.2)].

To account for the nonlinearity term let us introduce a multiplication coefficient (see Eq. (2.2) in Chapter 2)

$$\mu = \gamma \left[\exp\left(\int_0^d \alpha(E)\, dz \right) - 1 \right]$$

so that $j(t + \tau_i) \approx \mu j(t)$ is in accordance with the physical sense of $\alpha(E)$ (see, e.g., [Kudryavtsev and Tsendin, 2002]). In the case of slow evolution the Taylor expansion yields

$$\tau_i \partial_t j(t) \approx (\mu - 1) j(t), \tag{3.19}$$

where the self-sustain condition $\mu = 1$ is achieved for $E = E_b$ and is equivalent to (3.11). For a small overvoltage the multiplication coefficient is

$$\mu(E_b + \delta E) \approx \gamma(e^{\alpha_b d + \alpha_b' \delta U} - 1) \approx 1 + \alpha_b' \delta U$$

and the nonlinear term in (3.18) is restored from (3.19) up to the factor C_γ.

It is important to stress that (3.18) is applicable to slow (i.e., $\tau_i \partial_t \ll 1$) processes, correspondingly

$$\alpha_b' \delta U \ll 1 \tag{3.20}$$

that imposes a restriction on $U_s - U_b$. The standard approximation for the Townsend coefficient (2.3) is used

$$\alpha(E) = Ape^{-Bp/E}.$$

The value α' takes its maximal value at the inflection point (where $E = \frac{1}{2}Bp$) and quickly decreases with either an increase or decrease of the electric field, the maximal value of δU is $U_s - U_b$. Inequality (3.20) is ensured if

$$U_s - U_b \ll \frac{e^2 B}{4A}, \tag{3.21}$$

where the right-hand-side varies from 20 to 60 Volts for different gases. Condition (3.21) refines our original assumption (3.1).

Finally we rewrite (3.18) for the axial electric current density j

$$\partial_t j = D_a \nabla_\perp^2 j + C_\gamma \frac{\alpha_b' \delta U}{\tau_i} j \tag{3.22}$$

as determined by (3.12), and turn to the consideration of the high-ohmic barrier.

3.3 The high-ohmic barrier

In this section we derive the missing equation for the overvoltage $\delta U(x, y, t)$, which will turn out to be a linear partial differential equation. To begin with we note that the combination $\epsilon_0 \epsilon \partial_t E_z + j_z$ must be continuous at the gas-cathode interface so that

$$\left(\epsilon_0 \partial_t E_z + j\right)_{z=d-0} = \left(\epsilon_0 \epsilon \partial_t E_z + j_c\right)_{z=d+0}, \tag{3.23}$$

where the Townsend approximation for the electric current density j in the gas is given by (3.12), j_c is the axial current density in the cathode, and ϵ is the cathode dielectric constant. We consider the cathode as a simple linear conductor with the specific resistivity ρ, so that $j_c = E_z/\rho$. Now, the problem is reduced to the calculation of the axial electric field E_z. For the special case of a spatially uniform $\delta U(t)$ the field equals $(U_b + \delta U)/d$ in the gas and $(U_s -$

$U_b - \delta U)/d_c$ in the cathode. Inserting both fields in (3.23) we arrive at the standard approximation [Kolobov and Fiala, 1994a]

$$\mathfrak{c}\partial_t \delta U = \frac{U_s - U_b - \delta U}{\rho d_c} - j, \tag{3.24}$$

where the combination

$$\mathfrak{c} = \frac{\epsilon_0}{d} + \frac{\epsilon_0 \epsilon}{d_c} \tag{3.25}$$

is the cell capacity per unit area. It is also profitable to introduce characteristic cathode time

$$\tau_c = \rho d_c \mathfrak{c},$$

which is recognized as the RC time of the corresponding circuit. The last term in Eq. (3.25) usually dominates, τ_c reduces then to $\epsilon_0 \epsilon \rho$, i.e., to the Maxwell time of the cathode material. The interplay of τ_c and the ion travel time τ_i plays an important role in the following discussion.

Equation (3.24) is only the first approximation to the final equation for the overvoltage because the non-uniformity of δU was completely ignored. To take this non-uniformity into account we need an accurate solution of the Laplace equation with the corresponding boundary conditions. It can be given explicitly due to the small width of the discharge cell. Let us start with the gas region.

Note, that the electric potential at the metal contacts φ_A at $z = 0$ and φ_B at $z = d + d_c$ (see Fig. 3.1) can depend only on time, the difference $U_s = \varphi_A - \varphi_B$ is fixed and equal to the supply voltage. On the contrary, the potential φ_C at the gas-cathode interface at $z = d$ depends on all variables, but z. To get the electric field in a gas we have to solve the following problem

$$\nabla^2 \varphi = 0, \quad \varphi\big|_{z=0} = \varphi_A, \quad \varphi\big|_{z=d} = \varphi_C,$$

where the radial part of the Laplace operator is a small perturbation to the axial part. A corresponding solution is obtained as a perturbation expansion in the parameter d/R, where R is the characteristic transversal space scale of the radial structure in question. The electric potential in the gas reads as

$$\varphi = \varphi_A - \frac{z}{d}(\varphi_A - \varphi_C) - \frac{z^3 - zd^2}{6d}\nabla_\perp^2 \varphi_C$$

where the terms $\sim d^4/R^4$ are ignored. We insert $\varphi_A - \varphi_C = U_b + \delta U$ in the last equation and come to Eq. (3.5) for the radial electric field, whereas the axial field is given by

$$E_z = \frac{U_b + \delta U}{d} - \frac{3z^2 - d^2}{6d}\nabla_\perp^2 \delta U$$

in accordance with (3.4), i.e., we have

$$E_z\big|_{z=d-0} = E_b + \frac{\delta U}{d} - \frac{d}{3}\nabla_\perp^2 \delta U$$

or the boundary value of the electric field.

The electric field at the cathode is a solution of a similar problem

$$\nabla^2\varphi = 0, \quad \varphi\big|_{z=d} = \varphi_C, \quad \varphi\big|_{z=d+d_c} = \varphi_B,$$

where $\varphi_C - \varphi_B = U_s - U_b - \delta U$. It is easy to demonstrate that

$$E_z\big|_{z=d+0} = \frac{U_s - U_b - \delta U}{d_c} + \frac{d_c}{3}\nabla_\perp^2 \delta U.$$

We finally insert the electric fields in the boundary condition (3.23), omit small terms, and arrive at

$$\partial_t \delta U = D_c \nabla_\perp^2 \delta U + \frac{U_s - U_b - \delta U}{\tau_c} - \frac{j}{\mathfrak{c}}, \tag{3.26}$$

which is the desired extension of Eq. (3.24) for the overvoltage. Formally the combination

$$D_c = \frac{d_c^2}{3\tau_c}$$

can be considered as a diffusion coefficient; however the operator $\nabla_\perp^2$ originates from the radial component of the electric field and does not describe any real diffusion.

Equations (3.22) and (3.26) provide a self-consistent description of the physical system depicted in Fig. 3.1.

3.4 The reduced system

Let us introduce normalized variables

$$u = \frac{j}{j_0} \quad \text{and} \quad v = \frac{\delta U}{U_s - U_b},$$

and the dimensionless overvoltage parameter

$$s = C_\gamma \alpha_b' (U_s - U_b) \ll 1.$$

Parameter s shall be small in accordance with (3.20). We now rewrite (3.22) and (3.26) as a two-component reaction-diffusion system

$$\tau_u \partial_t u = d_u^2 \nabla_\perp^2 u + uv, \tag{3.27}$$

$$\tau_v \partial_t v = d_v^2 \nabla_\perp^2 v + 1 - u - v. \tag{3.28}$$

The system is our main result. It is somewhat similar to different qualitative models developed by several authors, but is quantitative, i.e., characteristic time scales

$$\tau_u = \frac{\tau_i}{s} \quad \text{and} \quad \tau_v = \tau_c,$$

τ_u	d_u	τ_v	d_v
$4.1 \cdot 10^{-6}\,\mathrm{s}$	$1.7 \cdot 10^{-2}\,\mathrm{cm}$	$9.7 \cdot 10^{-6}\,\mathrm{s}$	$5.7 \cdot 10^{-2}\,\mathrm{cm}$

Table 3.1: Typical parameters for the system (3.27, 3.28). The corresponding values of the discharge cell parameters are specified in the text.

and diffusion lengthes

$$d_u = \sqrt{\frac{\lambda_e d}{s}} \quad \text{and} \quad d_v = \frac{d_c}{\sqrt{3}},$$

can be quantitatively calculated for any system in question. For instance, let us assume that $d = d_c = 0.1\,\mathrm{cm}$, the gas is nitrogen, and the pressure $p = 1.33 \cdot 10^4\,\mathrm{Pa}$. Parameters A and B, particle mobilities, and diffusion coefficients can be found in [Raizer, 1991]. We take $\gamma = 0.02$ and obtain the breakdown voltage $U_b = 885\,\mathrm{V}$. The right-hand-side of Eq. (3.21) is $58\,\mathrm{V}$, so that we assume $U_s = 895\,\mathrm{V}$ that results in $s = 0.19$. For the cathode material we assume $\epsilon = 10$ and $\rho = 10^7\,\Omega\,\mathrm{cm}$ (e.g., a semiconductor wafer) that corresponds to $j_0 = 10^{-5}\,\mathrm{A/cm^2}$. The corresponding set of parameters for the system (3.27, 3.28) is given in the Table 3.1.

In general, the system dynamics are determined by two dimensionless ratios τ_u/τ_v and d_u/d_v, both quantities are of order unity in our example. Of course, either large or small ratios are also possible. In contrast to this, both u and v are always of order unity due to the normalization. The diffusion lengthes d_u and d_v shall be smaller than the radial space scale R, nonlinearity is hence superior to diffusion. Typically, most of the physical space is occupied with a homogeneous stationary solutions of Eqs. (3.27, 3.28). Diffusion is only important in transition regions where spatial dependence of u or v is essential, e.g., in the case of ionization fronts.

Notice that the system (3.27, 3.28) incorporates only radial coordinates and slow time evolution. All numerical coefficients in the system can be quantitatively calculated, that is, our predictions can be compared with experimental data.

The derived set of Eqs. (3.27, 3.28) is much better suited for an analytical and numerical investigation of systems as that depicted in Fig. 3.1 than the full drift-diffusion set of equations. In particular, in Eqs. (3.27, 3.28) the solution in full 3-dimensional space has to be implemented numerically only for two space coordinates because the axial dependence is taken into account analytically.

Solutions of the basic system (3.27, 3.28) are systematically discussed in the next chapter.

Chapter 4

Front propagation into an unstable state

In this chapter the properties of the reduced two-component reaction-diffusion system are investigated. Section 4.1 deals with stationary states and uniform breakdown whereas in section 4.2 ionization fronts being nontrivial solutions of the system in question are discussed in details. In particular velocity and initial condition selection are studied in one- and two spatial dimensions.

4.1 Stationary solutions and their stability

4.1.1 Stationary states and ionization waves

For the sake of simplicity first of all let us introduce dimensionless time $t := t/d_v$ and space variables $x := x/d_v$ and rewrite the system (3.27, 3.28) obtained in the last chapter in the form

$$\begin{aligned} \tau u_t &= d^2 \nabla_\perp^2 u + uv \\ v_t &= \nabla_\perp^2 v + 1 - u - v, \end{aligned} \tag{4.1}$$

where as before $u = u(x, y, t)$ and $v = v(x, y, t)$ are normalized current density and normalized overvoltage respectively, $\nabla_\perp^2 = (\partial_x, \partial_y)$. The constant d^2 denotes a ratio of the diffusion lengths $d = d_u^2/d_v^2$, whereas τ represents a ratio of the characteristic time scales and $\tau = \tau_u/\tau_v$.

The system (4.1) has two stationary homogeneous equilibrium solutions. The solution ($u = 0$, $v = 1$) corresponds to a vanishing current and peak overvoltage, and is referred to as the *overvoltage state*. The second solution ($u = 1$, $v = 0$) describes a stationary *Townsend state*. As explained in the previous Chapter 3, the system is assumed to be near the breakdown point when the supply voltage is suddenly increased to a value $U_s > U_b$. A corresponding initial condition for Eqs. (4.1) is $u = v = 0$. An initial stage of the system evolution is described by the exact partial solution with $u \equiv 0$ and

$$\tau_v \partial_t v = d_v^2 \nabla_\perp^2 v + 1 - v,$$

which physically corresponds to the condenser charging. The system reaches the overvoltage state, which, of course, is unstable. Assuming a small harmonic perturbation of the overvoltage state $u = 0 + \widetilde{u}$, $v = 1 + \widetilde{v}$ with the perturbation terms $\sim \exp(ikx + \Gamma t)$, we reduce Eqs. (4.1) to a dispersion relation for Γ,

$$\Gamma^2 + \left(\frac{d^2k^2 - 1}{\tau} + k^2 + 1\right)\Gamma + \frac{d^2k^4 + (d^2 - 1)k^2 - 1}{\tau} = 0$$

There are two real roots

$$\Gamma_1 = \frac{-d^2k^2 + 1}{\tau} \quad \text{and} \quad \Gamma_2 = -k^2 - 1,$$

where the first root indicates an instability. If $\tau < 1$, the instability develops immediately after an increase of the supply voltage and the overvoltage state is not really achieved. The instability corresponds to the breakdown and brings the system to the Townsend mode of operation. The latter is asymptotically stable. Indeed, we start from the Townsend state, add a small perturbation $u = 1 + \delta u$, $v = 0 + \delta v$ proportional to $\exp(ikx + \Gamma t)$, and arrive at the dispersion relation

$$\Gamma^2 + \left(1 + \frac{(d^2 + \tau)k^2}{\tau}\right)\Gamma + \frac{d^2k^4 + d^2k^2 + 1}{\tau} = 0.$$

One can check that $\operatorname{Re}\Gamma < 0$ for all k. If in addition $\operatorname{Im}\Gamma \neq 0$, the perturbation oscillates in space and time and can be interpreted as a decaying *ionization wave*. By analyzing the $\operatorname{Im}(\Gamma)$ it is shown that this happens if $\tau < 4$.

We stress that the above solutions correspond to a small perturbation of the stationary states, i.e., to linear waves. Essentially nonlinear solutions appear if we consider a dynamical transition from the overvoltage state to the Townsend state. The details of such a transition can be surprisingly different depending on the system parameters. These solutions are investigated below.

4.1.2 Uniform solutions

An important class of solutions of Eqs. (4.1) is generated if the discharge is uniform in space, i.e.,

$$\tau_u \dot{u} = uv, \tag{4.2}$$

$$\tau_v \dot{v} = 1 - u - v, \tag{4.3}$$

so that the basic system can be replaced by an equivalent second order equation

$$\tau_u \tau_v \ddot{v} + (\tau_u - \tau_v v)\dot{v} + v - v^2 = 0,$$

where the dot denotes derivation with respect to time. The equation describes a uniform transition from the overvoltage state to the Townsend state.

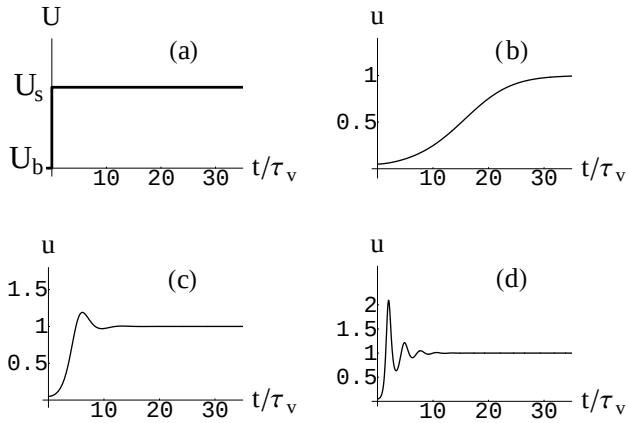

FIG. 4.1: Numerical results for temporal behavior of $u = j/j_0$ for uniform breakdown [Eqs. (4.2,4.3)]. Initial conditions are $u(0) = 0.05$ and $v(0) = 0.0$, i.e., the initial current fluctuation is 5% of the final value. (a) applied voltage, arbitrary units; (b) $\tau = 5$, no oscillations; (c) $\tau = 1$, the current profile is non-monotonic; (d) $\tau = 0.2$, damping current oscillations.

For $\tau > 4$ the current increases monotonically. As above, if either the circuit capacity or resistivity are large enough and $\tau < 4$ the discharge current is subject to damped oscillations.

Figure 4.1 shows the electric current behavior for different values of τ. It should be noted, that the uniform breakdown requires homogeneous initial perturbation (i.e., uniform distribution of seed electrons) that is highly unlikely. A more realistic picture corresponds to a small initial current fluctuation induced locally in space by a group of seed electrons or by a local inhomogeneity of electrodes. It is then necessary to consider nonuniform solutions of Eqs. (4.1).

4.2 Ionization fronts

The non-uniform breakdown, as a possible solution of Eqs. (4.1), occurs in the form of *ionization fronts*. They turn out to be transition waves between unstable and stable system states. As was mentioned in section 1.1, the fronts propagate along the electrodes, their form depends on system parameters but not on the seed fluctuation. In the literature propagation of such fronts is often referred to as *a front propagation into unstable state* [Murray, 1993, Ebert and van Saarloos, 2000, van Saarloos, 2003].

Such fronts arise in different physical systems. Here we only mention Taylor [Ahlers and Cannell, 1983] and Rayleigh-Bénard [Fineberg and Steinberg, 1987] convections, transient microstructures in strucural phase transitions [Salje, 1993] or dielectric breakdown fronts [Ebert et al., 1996]. Although

most of the fronts mentioned above are described by a one-component nonlinear diffusion equation, two component models can also be found [Ebert et al., 1996, Ebert and van Saarloos, 1997, Theodorakis and Leontidis, 2002].

Now our goal is to analyze the propagating ionization fronts, resulting from the system (4.1) as well as to determine, which class ionization fronts belong to and find the propagating velocity. We discuss these problems below, starting with the case of one spatial dimension.

4.2.1 Ionization fronts in 1D

Although our basic system is much more easy to treat than the original discharge Eqs. (3.6,3.7), there are no analytical solutions in the general case of Eqs. (4.1) and the numerical solutions are instead referred to. A small local initial current fluctuation leads to an exponential increase in the current. Furthermore, the instability develops in a nonlinear way: an ionization front propagates away from the initial perturbation. Finally the uniform state with $j = j_0$ ($u = 1$, $v = 0$) is established on the whole electrodes area, but plasma edges where boundary conditions affect the final current distribution.

Four typical examples of front behavior for different parameters d and τ of the system are shown in Fig. 4.2. Space-time plots for the u-component are presented in the left column, whereas the right column shows the u (red curve) and v (blue curve) components for a given time. One can see that in addition to monotonic fronts (Fig. 4.2 (a)), oscillating fronts can be observed (see Fig. 4.2 (b,c,d)).

More complicated scenarios appear if there is more than one initial fluctuation. An example of such behavior can be seen in Fig. 4.3. Several fronts are produced, they collide and merge with each other in the course of the collision process. At the end, however, we always have only one front that transforms the system into the uniform Townsend state.

Numerical simulations of the system (4.1) show that the evolution to the stationary Townsend state ($u = 1$, $v = 0$) can be either monotonic or oscillatory. So, our next goal is to determine for which system parameters (d and τ) the system produce these regimes. To this end let us move to a frame moving with a constant velocity $\xi = x - ct$,

$$d^2 u_{\xi\xi} + \tau c u_\xi + uv = u_t$$
$$v_{\xi\xi} + c v_\xi + 1 - u - v = v_t,$$

where $u = u(\xi, t), v = v(\xi, t)$.

Let us consider a stationary solution of this system and a small perturbation of the stationary solution $\widetilde{\mathbf{u}} = (\widetilde{u}, \widetilde{v})$, i.e., $u = 1 + \tilde{u}$, $v = 0 + \tilde{v}$. Then the equation for $(\widetilde{u}, \widetilde{v})$ becomes:

$$d^2 \widetilde{u}_{\xi\xi} + \tau c \widetilde{u}_\xi + \widetilde{v} = 0$$
$$\widetilde{v}_{\xi\xi} + c \widetilde{v}_\xi - \widetilde{u} - \widetilde{v} = 0,$$

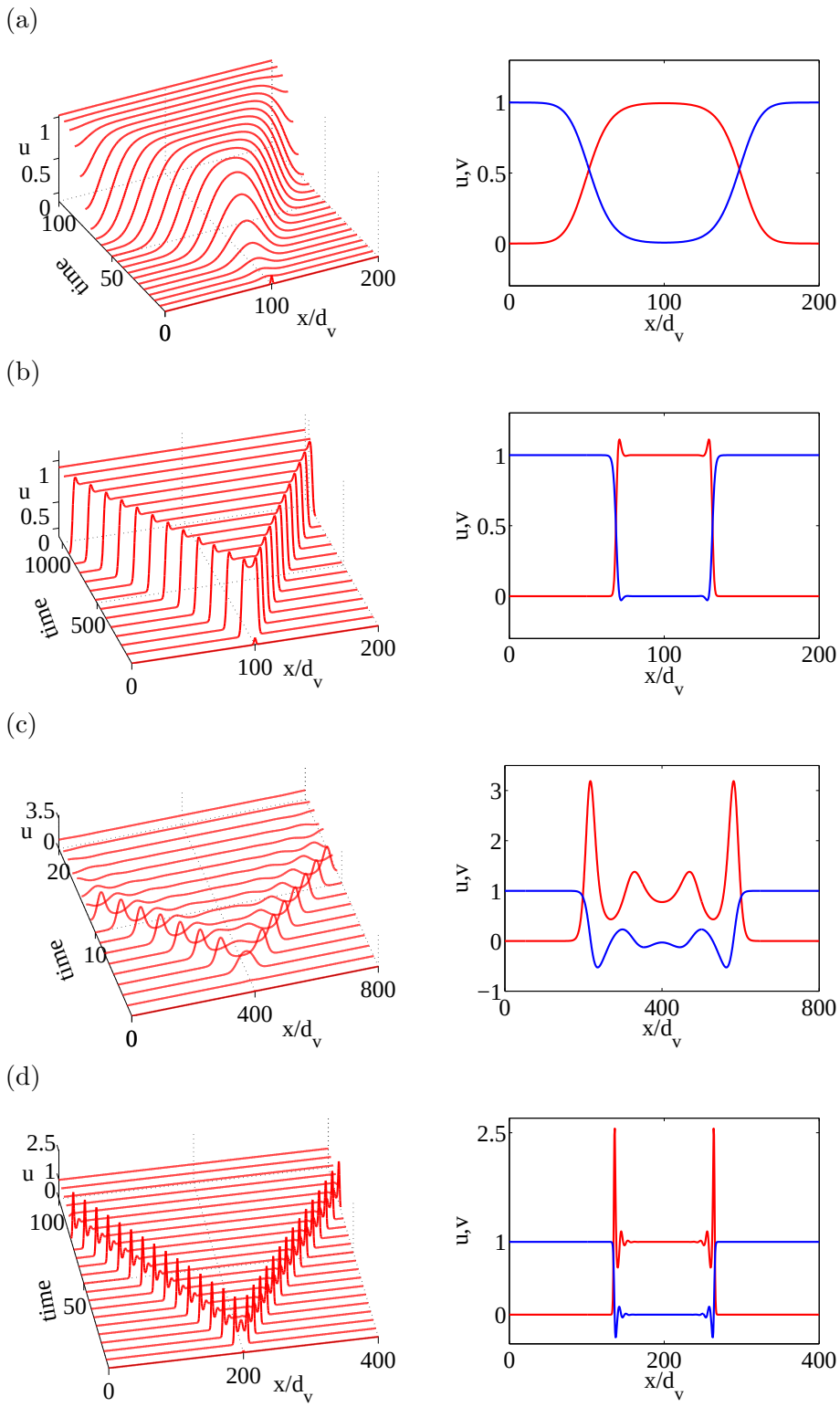

FIG. 4.2: Numerical results [Eqs. (4.1)] for the form of ionization fronts for different system parameters. u (red curve) and v (blue curve)components are presented. (a) $\tau = 5$ and $d = 4$, i.e., both time and space scales are determined by the gas; (b) $\tau = 5$ and $d = 0.25$, the cathode is adiabatic and diffusion in the gas can be ignored; (c) $\tau = 0.2$ and $d = 4$, the discharge is adiabatic and formal diffusion in the cathode can be ignored; (d) $\tau = 0.2$ and $d = 0.25$, both time and space scales are determined by the cathode. In all cases the Neumann boundary conditions were used. We started from $u = v = 0$ and added a small fluctuation of u at the origin. The fluctuation quickly changes to a stable front.

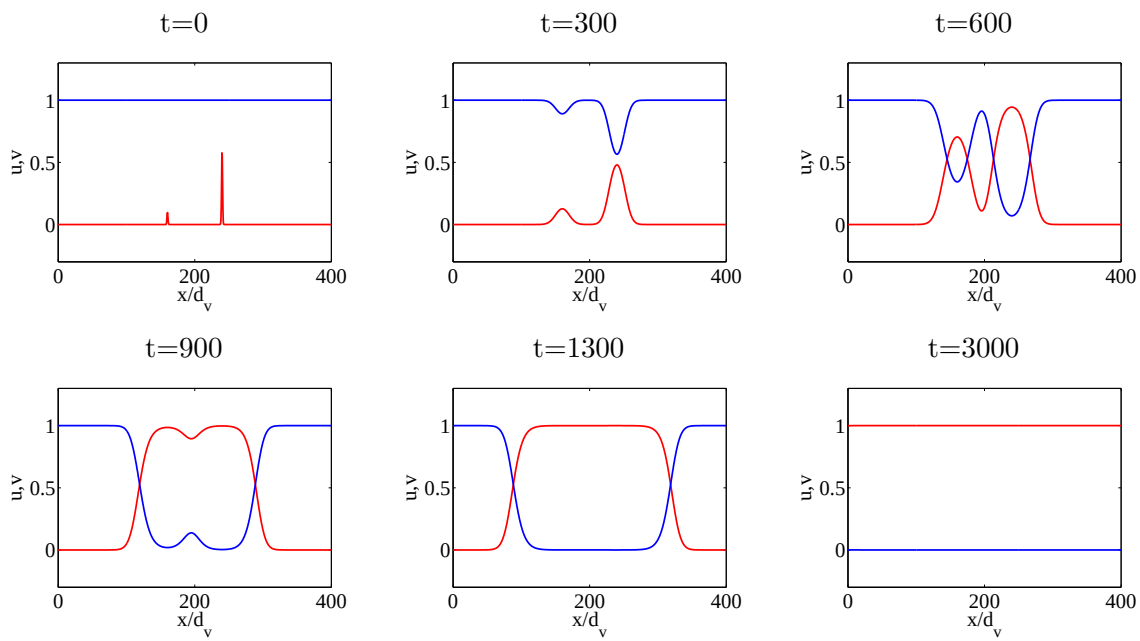

FIG. 4.3: A time evolution of the one-dimensional ionization front in the case that more than one initial fluctuation is presented. u (red curve) and v (blue curve) components are to be seen. Several fronts are produced, they collide and merge with each other in the course of collision processes. At the end, however, one has only one front that transforms the system in the stable state $u = 1$, $v = 0$. Parameters of the system are the same as in Fig. 4.2 (a).

After decomposing $\widetilde{\mathbf{u}}$ into modes $\widetilde{\mathbf{u}} \sim \mathbf{a}e^{\lambda\xi}$, $\lambda \in \mathbb{C}$ we get the equation

$$A_\lambda \mathbf{a} = 0 \tag{4.4}$$

with

$$A_\lambda = \begin{pmatrix} \lambda^2 d^2 + \tau c\lambda & 1 \\ -1 & \lambda^2 + c\lambda - 1 \end{pmatrix}.$$

The system (4.4) allows for a nontrivial solution if a compatibility condition

$$\det(A_\lambda) = d^2\lambda^4 + c(d^2+\tau)\lambda^3 + (\tau c^2 - d^2)\lambda^2 - \tau c\lambda + 1 = 0 \tag{4.5}$$

holds. This equation is a polynomial of the fourth order, so it can possesses at most four roots, which, depending on coefficients, can be either complex or real. If $\mathrm{Im}(\lambda) = 0$ the ionization front is monotonic and is oscillatory otherwise. So, if we know the velocity for given d and τ one can define the front behavior, analyzing $\mathrm{Im}(\lambda)$.

In order to calculate the front velocity numerically, one can, for example, derive the current as an integral of the $u = j/j_0$ over a space. Then one can obtain the front velocity as time derivative of this integral. An example of four typical front velocities corresponding to four different front types is shown in Fig. 4.4. One can see that for different system parameters the front velocity are of two orders of magnitude. Moreover, oscillating fronts move faster than monotonic fronts.

Calculating the front velocity for each pair (d, τ) the so-called *field of velocities* can be obtained (see Fig. 4.5). Figure 4.5 (a) shows the velocity field as a surface, whereas Fig.4.5 (b) represents it as a contour plot with a logarithmic τ-axis. One can see that for relatively large d and small τ values the velocity is much greater (in two orders of magnitude) than for the rest of the parameter space.

Now, having at disposal the field of velocities, i.e., the velocity of the ionization front for given (d, τ), one can go back to Eq. (4.5) to find parameter regions for monotonic as well as for oscillating fronts. So, as mentioned above, one can solve Eq. (4.5) for each (d, τ, c) and analyze the imaginary part of the solution. The result is shown in Fig. 4.6. The grey region corresponds to the case $\mathrm{Im}(\lambda) = 0$, i.e., monotonic fronts, whereas the white area meets a condition $\mathrm{Im}(\lambda) \neq 0$, what corresponds to the oscillatory behavior.

This result is in accordance with our intuitive idea about the front velocity. Indeed, as we mentioned above, the oscillatory fronts seem to have a tendency to move faster as monotonic fronts (see Fig. 4.4). In addition, as Fig. 4.5 shows, the large velocities are to expect in regions with relatively small τ, that corresponds in Fig. 4.6 to the region of existence of oscillatory fronts.

Although the velocity of the ionization front is simple to find numerically, the question arises, whether some analytical results can be obtained? This problem is discussed in detail in the next subsection.

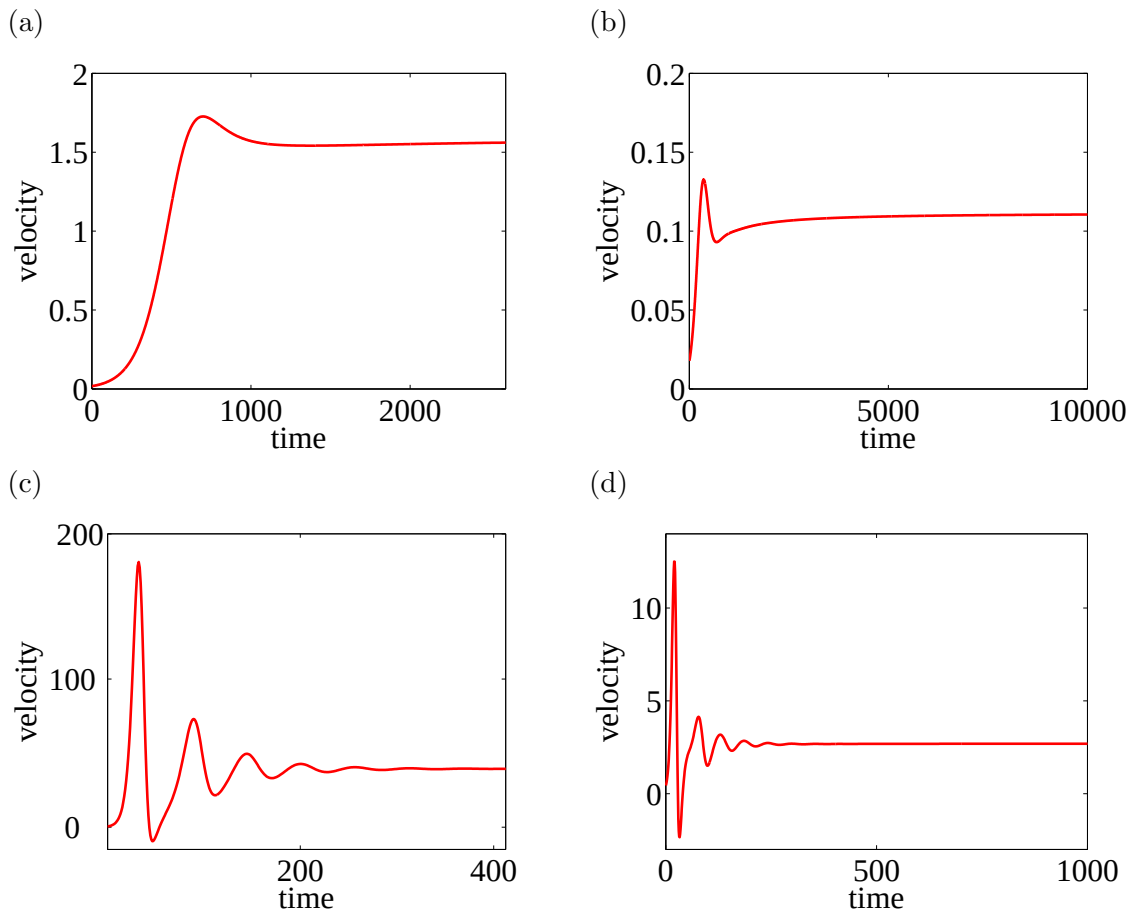

FIG. 4.4: Velocities of ionization fronts calculated for four typical front forms as a function of a time: (a) $d = 4$, $\tau = 5$, monotonic front; (b) $d = 0.25$, $\tau = 5$, one oscillation peak; (c) $d = 4$, $\tau = 0.2$, fast oscillating front; (d) $d = 0.25$, $\tau = 0.2$, oscillating front. Initially the front velocity increases in time, what corresponds to the region, where the ionization front is formed. After the front formation the velocity converges to the constant value, depending on system parameters.

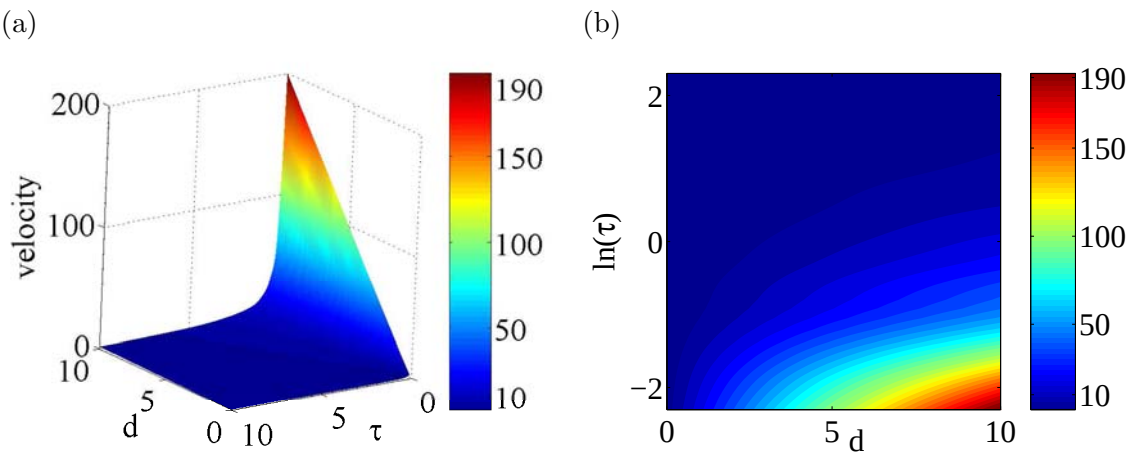

FIG. 4.5: Velocity fields calculated for different d and τ. (a) Velocity field as function of d and τ. (b) contour plot of the field: the $y = \tau$-axis logarithmic to better visualise the details for large d and small τ.

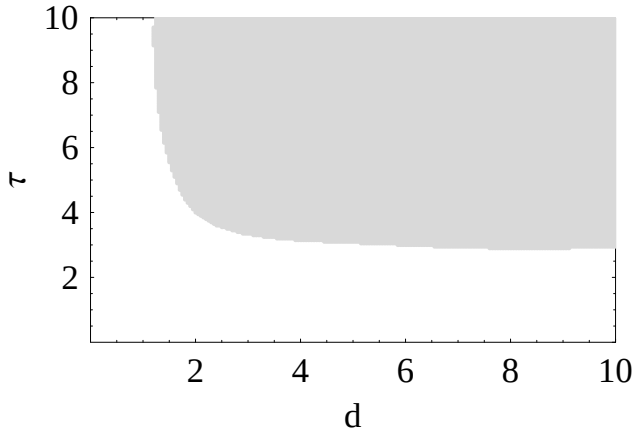

FIG. 4.6: Numerically calculated boundary as a function of d and τ, separating domains, corresponding to monotonic and oscillatory fronts. The grey domain corresponds to the region where monotonic fronts exist, whereas the white domain represents the area where oscillatory fronts are to be found.

4.2.2 Velocity and initial condition selection mechanism

Suppose that initially the system is in an unstable state except of some spatially localized region. The question is, what will be the long-time ($t \to \infty$) dynamical properties and velocity of the nonlinear front which will propagate into the unstable state? Are there classes of initial conditions for which the front converges to some unique asymptotic state c^*? If so, what can be said about the asymptotic front properties and convergence to them?

To address these questions, let us linearize the basic system (4.1) about the unstable state $u = 0, v = 1$. The linearized system reads:

$$\begin{aligned} \tau \widetilde{u}_t &= d^2 \widetilde{u}_{xx} + \widetilde{u} \\ \widetilde{v}_t &= \widetilde{v}_{xx} - \widetilde{u} - \widetilde{v}, \end{aligned} \tag{4.6}$$

where $(\widetilde{u},\ \widetilde{v})$ are the small perturbations of $u = 0,\ v = 1$, i.e., $u = 0 + \widetilde{u},\ v = 1 + \widetilde{v}$. From this point on we will have to deal only with the first equation of (4.6), because it is not coupled with $\widetilde{v}$, i.e., with

$$\tau \widetilde{u}_t = d^2 \widetilde{u}_{xx} + \widetilde{u}. \tag{4.7}$$

This equation is a linear diffusion equation with a source term, well known in the literature. Moreover, Eq. (4.7) is identical to the linearization of the classical nonlinear diffusion equation investigated by Fisher and Kolmogorov [van Saarloos, 1989, Ebert and van Saarloos, 2000, van Saarloos, 2003]. So one can try to apply the classical methods and results to the system (4.1).

Due to linearity of Eq. (4.7) for long times the profile in the leading edge will take the form $\widetilde{u} \sim \exp(ikx - i\omega t)$, where $\omega = \omega(k)$ is a dispersion function,

$$\omega(k) = \frac{\imath(1 - d^2 k^2)}{\tau}. \tag{4.8}$$

Notice that k and $\omega(k)$ can be complex: $k_i := \mathrm{Im}(k)$ is associated with the spatial decay of the front envelope and $k_r := \mathrm{Re}(k)$ with the oscillations, since $\mathrm{Re}(e^{\imath kx}) = e^{-\mathrm{Im}(kx)} \cos\big(\mathrm{Re}(kx)\big)$.

Since k is in general complex, the dynamical selection of both its real and complex parts must be analyzed. The selection of a particular "mode" $\mathrm{Re}(k)$ can be understood as follows: For fixed values of $k_i = k_{i0}$ the growth rate $\omega_i := \mathrm{Im}(\omega(k))$ is a function of k_r only and has a maximum at $k_r = 0$ as shown in Fig. 4.7 (a). Hence if one considers a superposition of profiles of the form $\exp(ikx - i\omega t)$ with the same value of the spatial decay $k_i = k_i^\dagger$, the long-time appearance of the profile will be dominated by the mode k_r corresponding to the $\max(\omega_i)$, i.e., for which $\partial\omega_i/\partial k_r = 0$ and $\partial^2\omega_i/\partial k_r^2 < 0$. So, in order to understand the selection of the spatial decay rate k_i it is enough to consider for each value of k_i only the maximum rate mode. In other words, k_r is considered to be an implicit function of k_i through the condition $\partial\omega_i/\partial k_r = 0$.

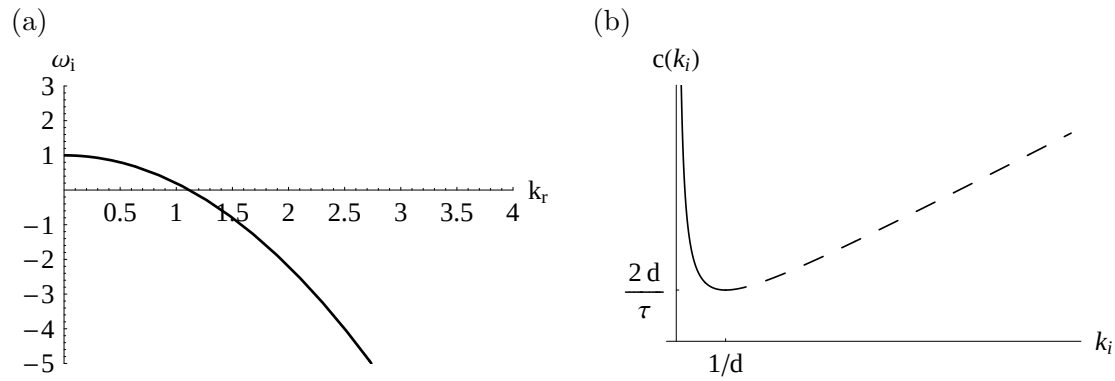

FIG. 4.7: (a) The growth rate ω_i as function of k_r by a fixed spatial decay k_i; (b) Behavior of the front envelope velocity, k_r is an implicit function of k_i, so $c = c(k_i)$.

Thus the envelope velocity

$$c := c(k_i) = \frac{\omega_i}{k_i} = \frac{1}{\tau k_i} + \frac{d^2 k}{\tau} \tag{4.9}$$

is the function of k_i only (see Fig. 4.7 (b)). As can be seen from Eq. (4.9) and Fig. 4.7 (b) the envelope velocity is a parabola with a minimum at $k_i^{min} = 1/d$.

Let us first check the stability of both parabola branches described by Eq. (4.9). For this aim we move to the frame moving with the envelope velocity $\xi = x - ct$. In this frame Eq. (4.7) reads

$$\tau \widetilde{u}_t = d^2 \widetilde{u}_{\xi\xi} + \tau c \widetilde{u}_\xi + \widetilde{u}.$$

In the leading edge region $\widetilde{u} \sim \alpha(t) \exp(-k_i \xi)$, where the spatial decay $k_i \geq 0$, so one obtaines

$$\dot{\alpha}(t) = \left(\frac{d^2}{\tau} k_i^2 - c k_i + \frac{1}{\tau} \right) \alpha(t).$$

Then the stability conditions for c are

$$k_i \geq 0$$
$$f(k_i, c) = \frac{d^2}{\tau} k_i^2 - c k_i + \frac{1}{\tau} \leq 0;$$

It is easy to show that the latter conditions are satisfied if $f(k_i^*, c) \leq 0$, where $k_i^* = c\tau/2d^2$ is a minimum of the function $f(k_i, c)$. In its turn, the inequality $f(k_i^*, c) \leq 0$ is satisfied if and only if $c \geq 2d/\tau$. Thus, the envelope velocity is stable only on the left branch of the parabola (4.9), i.e., for $k_i \leq 1/d$. This region of stable velocities is depicted in Fig. 4.7 (b) as a solid line, whereas the dotted line shows the unstable velocities for $k_i > 1/d$. The following discussion concentrates on the left branch of the solutions.

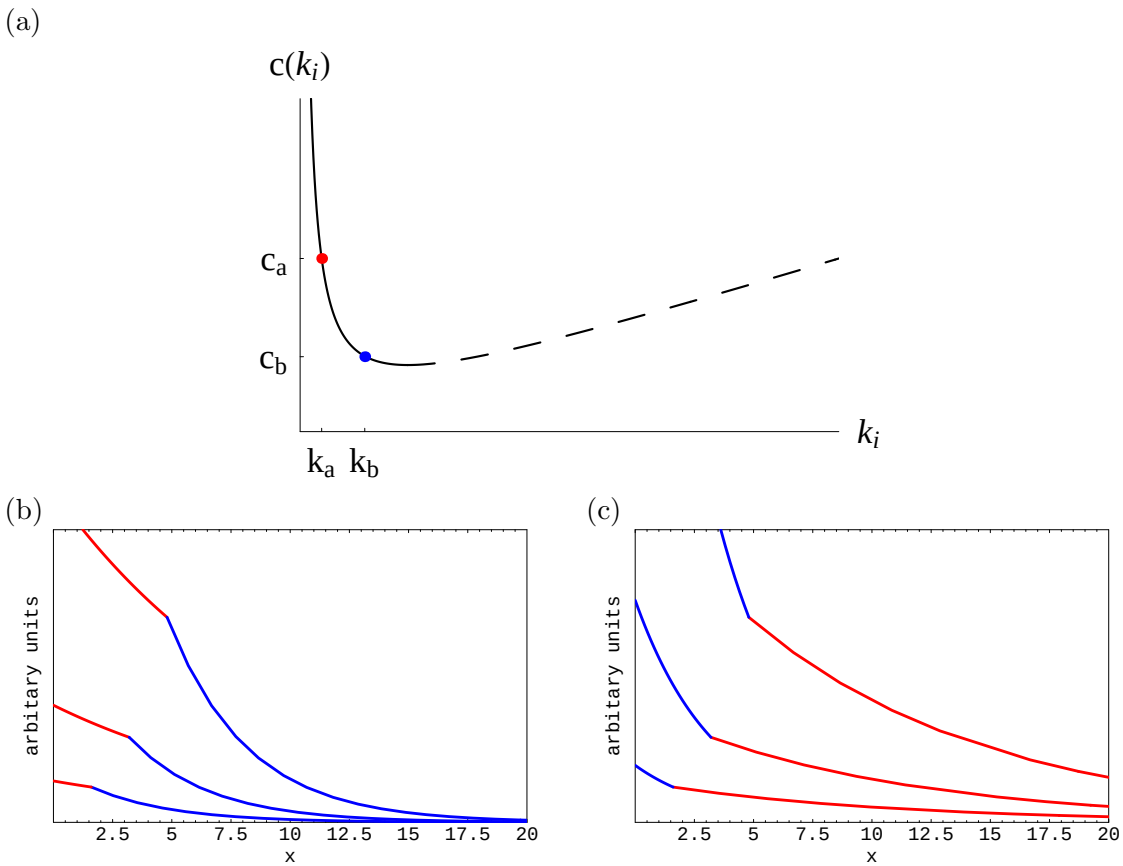

FIG. 4.8: Intuitive illustration of velocity selection. (a) Typical behavior of $c(k_i)$. The behavior of the fronts, corresponding to points $(k_a,\ c_a)$ and $(k_b,\ c_b)$ are shown in figures (b) and (c); (b) The lower part of the envelope of a front profile, drawn with a blue line corresponding to the point $(k_b,\ c_b)$ in figure (a). It moves slower as a red line, corresponding to $(k_a,\ c_a)$, but falls off steeper. The figure demonstrates how the crossover point moves higher with time, so that the profile becomes dominated by the slowly moving part; (c) If the slowest profile with $(k_b,\ c_b)$ is not one to the right, the fastest profile emerges.

To understand the essence of the dynamical mechanism of the velocity selection let us imagine a hypothetical front consisting of two pieces of the form $\exp(\imath kx - \imath\omega t)$ with two different values of k_i and velocities c (see Fig. 4.8 (a)). As sketched in Fig. 4.8, the line drawn with a red line drops off slower than the blue piece, as $k_a < k_b$ (see Fig. 4.8 (a, b)). On the other hand, as Fig. 4.8 (a) indicates, the red profile moves faster than the blue ones ($c_a > c_b$). Nevertheless, as Fig. 4.8 (b) demonstrates, the slowest moving part of the profile expands in time, i.e., becomes dynamically dominant. That is, for $t \to \infty$ the velocity $c^* = 2d/\tau$, corresponding to the smallest wave number $k_i^{min} = 1/d$ is seems to be selected.

Notice, that this conclusion is based on two facts, namely (a) the fastest

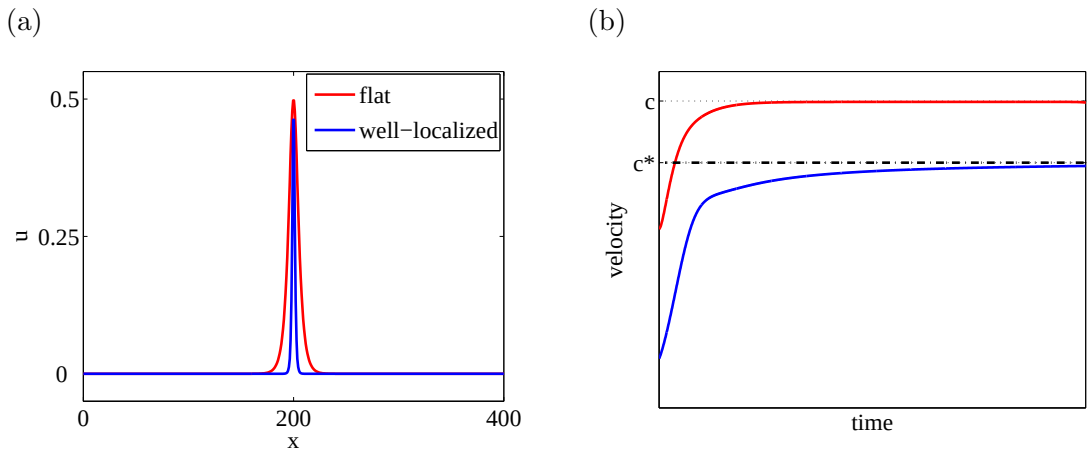

FIG. 4.9: Illustration of initial condition selection. (a) Two initial conditions, corresponding to sufficient-localized (blue distribution) and flat (red line) types are shown (b) Corresponding to both initial condition types asymptotic front velocities are to be seen. One can see that blue distribution results in front, moving with the minimal velocity c^*, whereas the red initial distribution leads to the front with velocity $c = c(\alpha) > c^*$. Parameters are: $d = 2$, $\tau = 5$.

profile has the slowest spatial decay and (b) the fact that the part with the fastest spatial decay is *to the right* of the one with the slower spatial decay. That is, the slowest profile dominates because it is in front of the faster one. Indeed, if both lines are interchanged so that the faster one is to the right, as shown in Fig. 4.8 (c), the faster one dominates the long-time dynamics.

These observations imply that initial conditions are important: only if the initial condition profile $u(x, 0)$ drops off faster than $\exp(-k_i^{min} x)$ the asymptotic front velocity is equal to the minimum value of (4.9), i.e., $c^* = 2d/\tau$. Otherwise, if $u(x, 0) \sim \exp(-\alpha x)$, where $\alpha \leq k_i^{min}$, the asymptotic velocity is simply

$$c = c(\alpha) = \frac{d^2\alpha}{\tau} + \frac{1}{\tau\alpha} > c^*.$$

In the former case the initial condition is refereed to as *sufficiently localized* whereas in the latter case they are said to be *flat* [Ebert and van Saarloos, 2000]. Figure 4.9 illustrate the initial condition selection. In Fig. 4.9 (a) two distributions, corresponding to sufficiently localized (blue line) as well as to flat (red line) initial conditions are shown. Figure Fig. 4.9 (b) demonstrates the asymptotic velocities for both cases. One can see that sufficient localized initial condition lead to a front moving with the velocity $c^* = 2d/\tau$, whereas the flat distribution results in a front with the velocity $c(\alpha) > c^*$, as is shown above.

In the following the initial conditions are assumed to be sufficiently local-

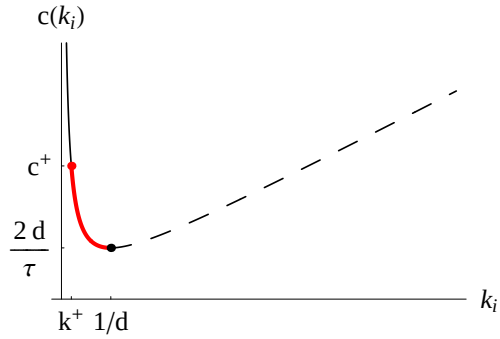

FIG. 4.10: Illustration of nonlinear marginal stability. The black solid line denotes the branch of solutions that are stable, whereas the solid red line denotes the branch that is unstable to the "invasion mode".

ized. In this case, as discussed above, the asymptotic velocity is given by

$$c^* = \frac{\omega_i}{k_i} = \frac{2d}{\tau}, \qquad \frac{\partial \omega_i}{\partial k_r} = 0, \qquad \frac{\partial^2 \omega_i}{\partial k_r^2} < 0. \tag{4.10}$$

These equations determine *the linear-marginal stable velocity* c^* as well as the wave number k_i^{min} at that point. The corresponding front is said to be *pulled* or *marginally stable* [Ben-Jacob et al., 1985, van Saarloos, 1989, Ebert and van Saarloos, 2000]. The analysis shows why the front velocity approaching the asymptotic value is based on the assumption that the dynamically relevant branch of $c(k_i)$ corresponds to the smallest root k_i^{min} for solving the equation (4.10). This occurs because an asymptotic spatial decay

$$\widetilde{u} \simeq \sum_j A_j(c) e^{-\imath k_i^j x}$$

will be dominated by the root with the smallest value of k_i, say, $k_i^{min} = k_i^1$, whenever the corresponding factor $A_1(c) \neq 0$. Nevertheless, it may happen that at some particular value $c^\dagger$ one has

$$A_1(c^\dagger) = 0, \tag{4.11}$$

so that asymptotic spatial decay is not given by $k_i^{min} = k_i^1$, but instead by the next root with $k_i^2 > k_i^1$. This situation is illustrated in Fig. 4.10. The dynamical implications of this can be understood immediately within the same context as those used for the case of linear marginal stability. Namely, the front moving with a velocity $c^\dagger$ drops off faster in space than any other front profile with velocity $c > c^*$. On the other hand if the velocity $c^\dagger$ satisfies Eq. (4.11), all fronts with $c < c^\dagger$ are unstable against "invasion" by the profile with $c^\dagger$ and the asymptotic front velocity for sufficient localized initial conditions becomes $c^\dagger$. So, $c^\dagger$ is also the velocity at which front profiles are *marginaly stable*. However, in this case the smallest root k_i^{min} does not dominate the asymptotic

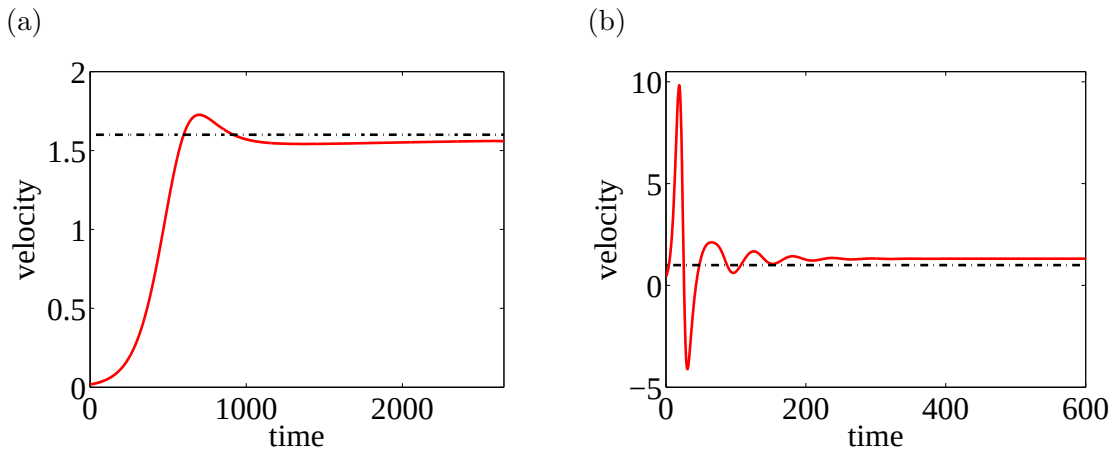

FIG. 4.11: Two front velocity types. (a) linear marginal stable velocity; (b) nonlinear marginal stable velocity; The asymptotic velocity c^* is marked by a dashed line. Parameters are: (a) $d = 4, \tau = 5$; (b) $d = 0.1$, $\tau = 0.2$.

spatial decay of the front profile and the asymptotic front behavior depends on the properties of the whole front. Therefore the velocity $c^\dagger$ is referred to as *the nonlinear marginal velocity* and the corresponding front profile is said to be *pushed* following [van Saarloos, 1989, Ebert and van Saarloos, 2000].

Although the physical understanding for the nonlinear marginal stability described above is quite simple, the analytical prediction of c^{dag} is much more complicated. However, sometimes it is possible to do for nonlinear diffusion equation with some spatial type of nonlinear term [van Saarloos, 1989]. For the system (4.1) we refer to a numerical solution. Figure 4.11 shows numerical examples of both velocity types. In Fig. 4.11 (a) a linear marginal stable velocity corresponding to the monotone front is shown. The asymptotic velocity c^* is marked by a dashed line. One can see, that the front velocity approaches the asymptotic state c^* from below (see also [Ebert and van Saarloos, 2000] for details). Figure 4.11 (b) shows another possible velocity regime, namely nonlinear marginal stable velocity, corresponding to the oscillatory front. One can see that the actual front velocity is constant and more than c^*.

The system (4.1) shows that both pulled and pushed fronts can be found. Numerical simulations show that monotonic fronts, occurring in (4.1) are pulled, whereas the oscillatory ones are pushed. In [Ebert and van Saarloos, 2000] it has been proven that for nonlinear diffusion equation monotonic fronts propagating with the asymptotic velocity c^* are stable, what is in agreement with our numerical results.

Notice that the linear marginal stable velocity c^* can also be found using saddle point approximation. Namely, a solution for the $\widetilde{u}(x,t)$ of Eq. (4.7) for

$t > 0$ can be written as the inverse Fourier transformation

$$\widetilde{u}(x,t) = \frac{1}{2\pi}\int_{-\infty}^{\infty} dk\, a_k e^{ikx - i\omega(k)t}, \tag{4.12}$$

where a_k is the Fourier transformation of the initial data $\widetilde{u}(x,0)$, i.e.,

$$\widetilde{u}(x,0) = \frac{1}{2\pi}\int_{-\infty}^{\infty} dk\, a_k e^{ikx},$$

and $\omega(k)$ is a dispersion. For Eq. (4.7) a dispersion relation can be easily obtained using the substitution $\widetilde{u} \sim e^{ikx - i\omega t}$:

$$\omega(k) = i(\frac{1 - k^2 d}{\tau}). \tag{4.13}$$

With the frame moving with the asymptotic velocity c^*, namely

$$\xi = x - c^* t,$$

the Eq. (4.12) takes the form

$$\widetilde{u}(\xi,t) = \frac{1}{2\pi}\int_{-\infty}^{\infty} dk\, a_k\, e^{ik\xi - i(\omega(k) - c^* k)t}. \tag{4.14}$$

To find c^* one should investigate the behavior of the last equation in the limit ξ *finite*, $t \to \infty$. The large-time limit clearly requires a *saddle-point approximation (stationary phase method).*

The concept of the method: When t tends to infinity we deform the k-contour to go through the point k^* in the complex k plane where the phase becomes stationary, i.e., the phase derivative with respect to k equals to zero. The integral is then dominated by the contribution from the region neighbouring this point.

For the integral (4.14) this *saddle (or stationary phase) point* k^* is given by

$$\left.\frac{d[\omega(k) - c^* k]}{dk}\right|_{k=k^*} = 0. \tag{4.15}$$

Additionally, the fact that the front moves with the asymptotic spreading velocity c^* means that neither exponentially growth nor decay on the right flank is seen. This requirement simply leads to

$$\mathrm{Im}[\omega(k^*) - c^* k^*] = 0. \tag{4.16}$$

For Eq. (4.7) the stationary phase point k^* and the linear spreading velocity c^* can be immediately obtained using the last two equations:

$$k^* = \imath\frac{\tau c^*}{2d^2} \qquad\qquad c^* = \frac{2d}{\tau} \tag{4.17}$$

Let us now summarize results obtained for the one-dimensional ionization fronts: Under certain system parameters the one-dimensional ionization fronts can be either monotone or oscillatory and move with a constant velocity. This velocity depends on front type and the initial distribution. Moreover, if the initial conditions are well-localized monotone fronts always move with the asymptotic marginal stable velocity c^*, which can be found analytically. In contrast, oscillatory fronts move with constant velocity $c^\dagger > c^*$, which are called to be nonlinear marginally stable and for the system in question can be found numerically. If the initial distribution is not sufficiently well-localized (flat) the front velocity depends on the initial distribution and system parameters. The case of two spatial dimensions is considered next.

4.2.3 Ionization fronts in 2D

As mentioned above, the system presented here is much more easy to solve than the original discharge Eqs. (3.6, 3.7). In particular, the information about whole 3D physical space can be obtained from calculating the (x, y, t) space only because the axial dependence can be taken into account analytically.

Qualitatively, the behavior of the general solution in two-dimensional space is the same as in one-dimension. An initial current perturbation changes to stable ionization front. The latter propagates away from the initial perturbation and quickly changes to a quasi-one-dimensional front. The structure of the transition region is also the same as in the one-dimensional case: apart from monotonic fronts, oscillatory behavior can also be found. An example of both front types is shown in Fig. 4.12, using the system parameters from Table 3.1. Figure 4.12 (a) shows a cross-section of the two-dimensional monotonic front for a fixed time moment. The red surface presents the $u = j/j_0$ distribution, whereas the blue surface describes the overvoltage v. An example of the oscillatory front is shown in Fig. 4.12 (b). As in the case of one dimension the fronts move with a constant velocity, that depends on system parameters and is independent on initial fluctuation if it is well-localized. In contrast to the one-dimensional front, the velocity in two-dimensions depends also on the front curvature. On the other hand, the two-dimensional front rather quickly changes to a quasi-one-dimensional front, moving with the asymptotic velocity c^* for monotonic and $c^\dagger$ for oscillatory fronts.

In the case of several initial fluctuations, the front behavior is also similar to the one-dimensional case: several fronts are produced, they collide and merge with each other throughout the collision process. At the end, however, there is only a single front that transforms the system into the uniform Townsend state. An example of the several ionization fronts is shown in Fig. 4.13 for monotonic fronts as well as in Fig. 4.14 for the oscillatory fronts. For both cases system parameters from the Table 3.1 were used.

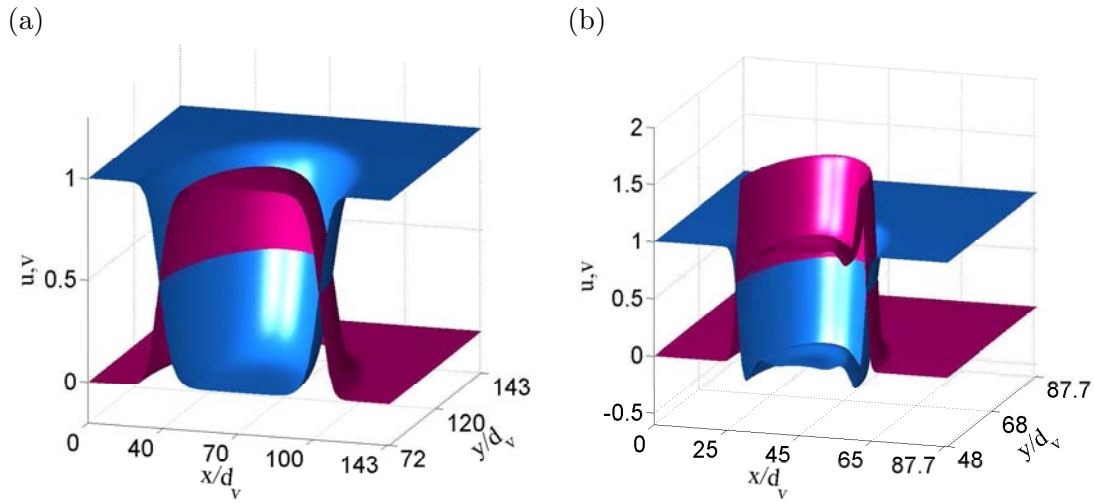

FIG. 4.12: Two dimensional ionization fronts. $u = u(x, y, t)$ (red) as well as $v = v(x, y, t)$ (blue) distributions are shown. (a) monotonic front, calculated at $t = 1500$. Parameters: $d = 5.2/3.5$, $\tau = 4.5/0.91$, $L = [0, 143] \times [0, 143]$, $dx = 0.01$, $dt = 0.03$; (b) oscillatory front, calculated at $t = 1100$. Parameters: $d = 1.7/5.7$, $\tau = 4.1/9.7$, $L = [0, 87.7] \times [0, 87.7]$, $dx = 0.01$, $dt = 0.03$. In both cases the Neumann boundary conditions were used.

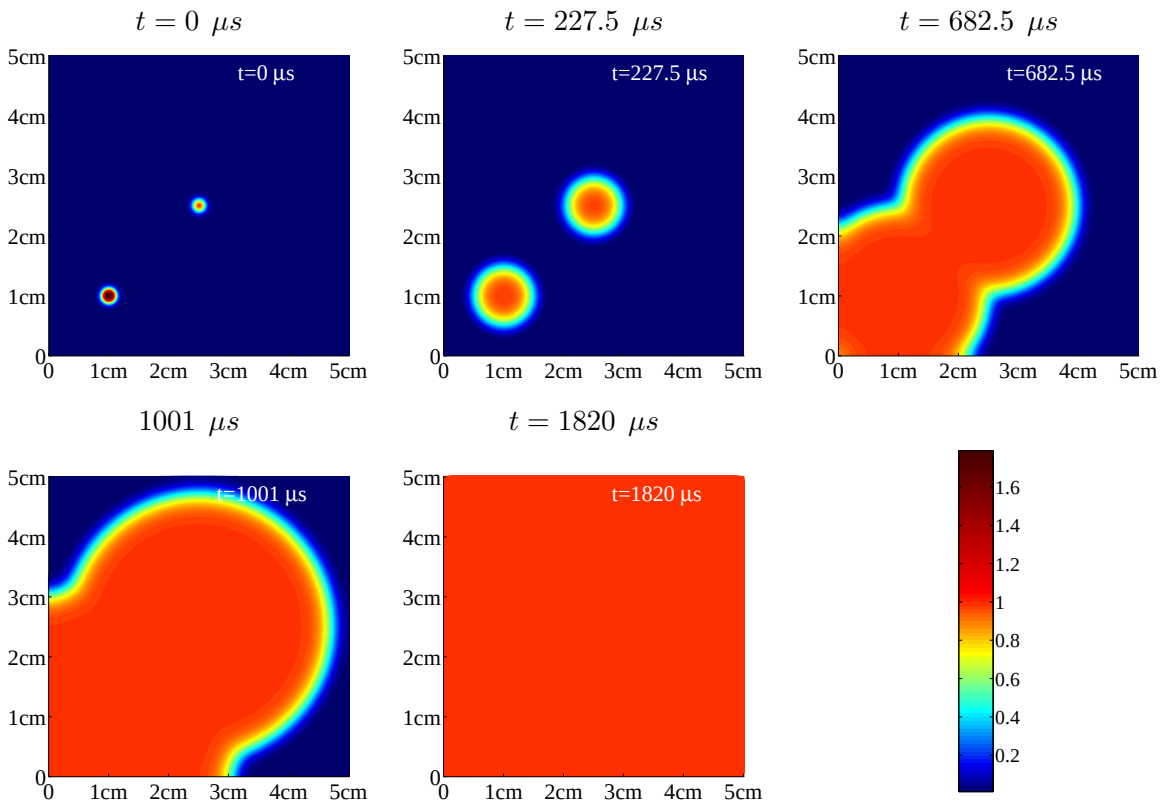

FIG. 4.13: Time evolution of several monotonic two-dimensional ionization fronts. Parameters are the same as in Fig. 4.12 (a).

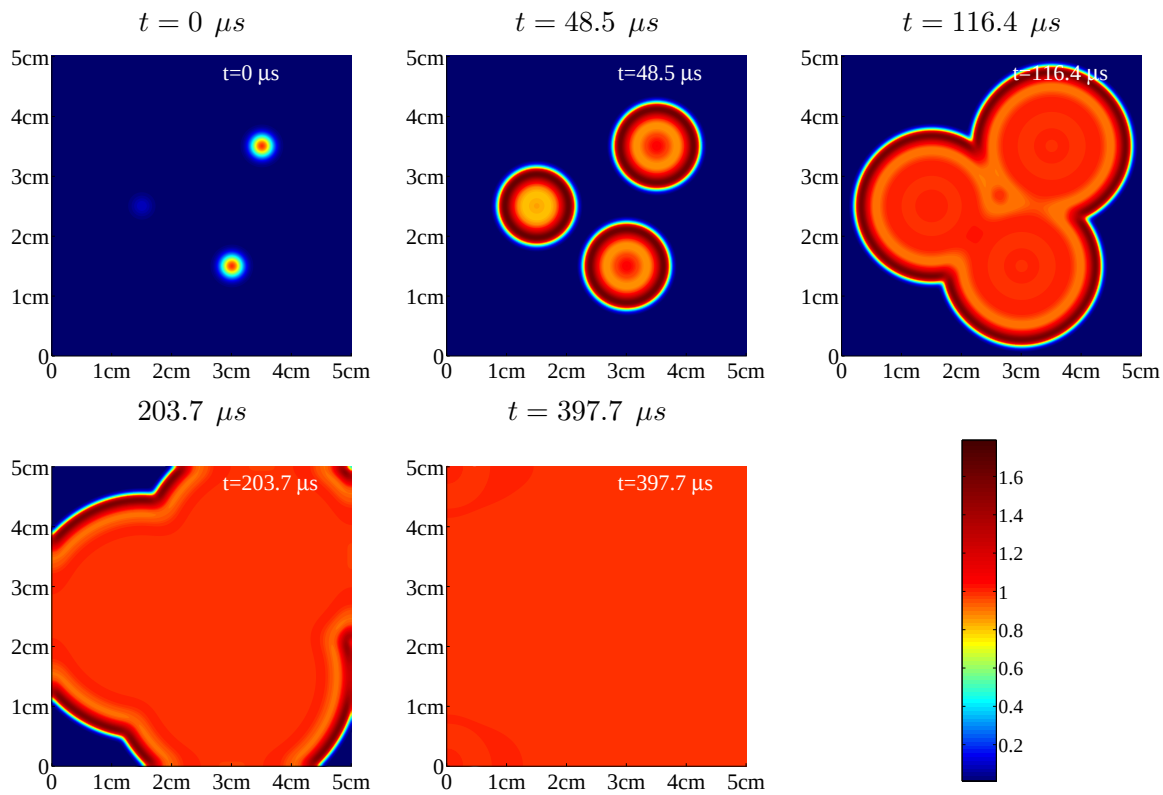

FIG. 4.14: Time evolution of several oscillatory two-dimensional ionization fronts. Parameters are the same as in Fig. 4.12 (b).

In conclusion, note that the key problem is that the experimental phenomena are observed on a macroscopic time scale (of the order of 10^{-3} s or longer), whereas the drift-diffusion approximation is on a microscopic time scale. A direct numerical solution of the full 3D drift-diffusion equations on macroscopical time scales is very time consuming or even impossible and a reduction of the drift-diffusion model is desirable. Such a reduction is developed using the fact that the axial dimension of the discharge cell in question is small as compared to the radial dimension [Amiranashvili et al., 2005]. Two-scale approach allows the axial and radial effects to be separated. The reduction is possible if the source voltage exceeds the breakdown voltage to only a small extent [Eq. (3.21)].

The drift-diffusion equations are simplified to a two-component *reaction-diffusion* system that incorporates only radial coordinates and slow time variation. All numerical coefficients in our system can be quantitatively calculated, that is, our predictions can be compared with experimental data.

The derived set of Eqs. (3.27,3.28) is much better suited for an analytical and numerical investigation of system depicted in Fig. 3.1 than the full drift-diffusion set of equations. In particular, in Eqs. (3.27,3.28) the solution in full 3-dimensional space has to be implemented numerically only for two space coordinates because the axial dependence is considered analytically.

Part II

Localized structures in three-component reaction-diffusion system

Chapter 5

Two- and three-component RD systems: phenomenological modeling

In this Chapter two- and three-component RD systems, being the phenomenological models for planar dc gas-discharge systems with a high ohmic semiconductor electrode are considered. Their solutions are briefly discussed.

As is mentioned in the Introduction in this Part a more complicated case of the experimental system operating in the glow mode is considered. This situation is much more complicated as compared to that in Part I, hence we use phenomenological modeling.

In [Radehaus et al., 1987], a gas-discharge system with a semiconductor electrode we are interested in has been described in terms of an equivalent electrical circuit from which a two-component reaction-diffusion has been obtained

$$\begin{aligned} \partial_t u &= D_u \Delta u + f(u) - \kappa_3 v + \kappa_1 - \kappa_2 \langle u \rangle, \\ \tau \partial_t v &= D_v \Delta v + u - v, \end{aligned} \tag{5.1}$$

where $\langle u \rangle$ denotes a spatial average, describing the global feedback effect, namely

$$\langle u \rangle = \frac{1}{|\Omega|} \int_\Omega u(r,t) dr. \tag{5.2}$$

Here Δ denotes the Laplace operator in one or two spatial dimensions, $f(u)$ is a nonlinear cubic-like function, e.g., $f(u) = \lambda u - u^3$ with $\lambda > 0$ (more general polynomial functions are also possible [Dohmen, 1991]). D_u, D_v denote the (positive) diffusion coefficients of the components, whereas the positive parameter τ represents a dimensionless constant, being the ratio of the characteristic times of v with respect to that of u.

One can consider the system 5.1 as an extension of the FitzHugh-Nagumo equations (see Chapter 1 for details). In addition, we note, that Eqs. (5.1)

describe an activator-inhibitor dynamic at least near the origin, because the activator $u = u(\mathbf{r}, t)$ stimulates the evolution of u and $v = v(\mathbf{r}, t)$, $\mathbf{r} \subset \mathbb{R}^1, \mathbb{R}^2$, while v inhibits both quantities. The model (5.1) has been derived for the system, where pattern formation is considered in $\mathbb{R}^1$ and $\mathbb{R}^2$ only. However, the case of $\mathbb{R}^3$ can also be considered.

According to this model, the activating component u is related to the avalanche multiplication of charged carriers in the discharge gap, while the voltage drop at the semiconductor plate plays the role of the inhibitor v. The constant κ_1 is connected with the normalized applied voltage and has arbitrary sign, whereas κ_2 is non-negative and describes a normalized internal resistance of the voltage source. Finally, κ_3, being a normalized strength of influence of v on u_t is also positive. A more detailed description explaining the physical meaning of the parameters can be found in [Bode et al., 2002, Purwins et al., 2005].

The model (5.1) serves for qualitative understanding of a wide variety of interesting experimentally observed phenomena in the gas-discharge system. In particular, super- and subcritical Turing and Hopf instabilities and their combination [Purwins et al., 1989, Heidemann et al., 1993, Dohmen, 1991], stationary, moving and interacting fronts as well as stationary, moving and breathing DSs [Willebrand et al., 1993a, Willebrand et al., 1993b, Bode and Purwins, 1995] in one spatial dimension can be mentioned. It is also possible to describe one or more stable stationary DSs in two and three dimensions and their bound states [Schenk et al., 1998], whereas single two-dimensional moving DS can be stabilized by a global feedback term ($\kappa_2 > 0$) [Krischer and Mikhailov, 1994]. However, the latter cannot suppress the growth of antisymmetric combinations of the unstable modes of two or more DSs, so that solutions with several moving and interacting pulses do not exist [Schimansky-Geier et al., 1991, Schenk et al., 1997]. On the other hand, multiple moving DSs are observed experimentally in planar gas-discharge system [Astrov and Purwins, 2001].

As is mentioned in the Chapter 1 the difficulties, connected with absence of solutions in form of several moving and interacting DSs can be overcome by introducing a second inhibiting component phenomenologically, say $w = w(\mathbf{r}, t)$ [Woesler et al., 1996, Schenk et al., 1997], which acts as a local feedback. The extended system reads:

$$\begin{aligned} \partial_t u &= D_u \Delta u + f(u) - \kappa_3 v - \kappa_4 w + \kappa_1, \\ \tau \partial_t v &= D_v \Delta v + u - v, \\ \theta \partial_t w &= D_w \Delta w + u - w. \end{aligned} \tag{5.3}$$

However, from the point of view of the gas-discharge physics, so far there are no strong arguments for adding a third inhibitor component to the system (5.1). On the other hand, w can be related to temperature or another characteristic of the high ohmic layer.

Nevertheless the system (5.3) allows to interpret various experimental phenomena that are not encountered in the model (5.1) such as several moving and interacting DSs, rotational bound states, influence of noise on the dynamic of DSs etc. [Or-Guil et al., 1998, Bode et al., 2002, Moskalenko et al., 2003, Gurevich et al., 2004b, Bödeker et al., 2003]. Note that the system (5.3) can be considered as a model system for the investigation of generic features of DSs and their interaction in non-linear RD systems.

In this thesis both models (5.1) and (5.3) are considered. We discuss the formation of one- and two-dimensional patterns arising as result of super- and sub-critical Turing instability in both models (see Chapter **??**). Properties and features of a single two-dimensional DS as a solution of (5.3) are also investigated. In the Chapter 7 we are concentrated on destabilization mechanisms leading to moving, breathing DSs and combination of both effects.